

# Asymptotically Normal Estimation of Local Latent Network Curvature

Steven Wilkins-Reeves <sup>\*1</sup> and Tyler McCormick <sup>†1,2</sup>

<sup>1</sup>Department of Statistics, University of Washington

<sup>2</sup>Department of Sociology, University of Washington

November 22, 2022

## Abstract

Network data, commonly used throughout the physical, social, and biological sciences, consist of nodes (individuals) and the edges (interactions) between them. One way to represent the complex, high-dimensional structure in network data is to embed the graph into a low-dimensional geometric space. Curvature of this space, in particular, provides insights about structure in the graph, such as the propensity to form triangles or present tree-like structure. We derive an estimating function for curvature based on triangle side lengths and the midpoints between sides where the only input is a distance matrix and also establish asymptotic normality. We next introduce a novel latent distance matrix estimator for networks as well as an efficient

---

\*stevewr@uw.edu

†tylermc@uw.edu

algorithm to compute the estimate via solving iterative quadratic programs. We apply this method to the Los Alamos National Laboratory Unified Network and Host dataset and show how curvature estimates can be used to detect a red-team attack faster than naive methods, as well as discover non-constant latent curvature in co-authorship networks in physics.

## 1 Introduction

Social networks consist of a set of actors and the connections between them. Formally, take a set of nodes (or vertices)  $V = \{1, 2, \dots, n\}$  and edges  $E \subset \{(i, j) | i \neq j, i \in V, j \in V\}$  and define a graph or network  $G = (V, E)$ . Beyond just the social network setting where these actors may represent individuals (e.g. Borgatti et al. (2009)), network models are used in many areas of the biological and physical sciences where the nodes may represent objects of interest such as cells (e.g. Bassett et al. (2018)), and particles (e.g. Papadopoulos et al. (2018)) respectively.

High-dimensional, complex structure is an inherent feature of network data. This structure creates challenges in representing and modeling these rich data. One common approach uses embedding into lower-dimensional geometric spaces, where both properties of the geometric space and the position of points in the space reveal insights about the structure in the graph.

In this paper, we focus on the properties of the geometric space and, in particular, the notion of curvature. Sectional curvature of a latent space is, broadly defined, the deviation from a flat (Euclidean) space via the growth of the circumference of small circles as a function of their radius. Numerous previous approaches in this area have adopted a “discrete” approach, where the discreteness arises from the structure of the distance matrix between nodes (e.g. using path length). These curvature definitions include Ollivier-Ricci Curva-

ture (Ollivier, 2007), Haantjes-Ricci curvature (Saucan et al., 2020) and Forman-Ricci curvature (Leal et al., 2018). Despite some of their unknown statistical properties, these ideas have been useful in a variety of applications such as understanding financial network instability (Sandhu et al., 2016; Samal et al., 2021), network sampling (Barkanass et al., 2022), cancer detection in gene regulatory networks (Sandhu et al., 2015), functional neuroscience (Farooq et al., 2019) and community detection (Sia et al., 2019; Ni et al., 2019). These definitions are motivated for networks defined as a static object, and do not necessarily measure the curvature of the latent space. Therefore it is not obvious what an estimate will be converging to when a network is studied as a random object.

Our approach deviates from these previous approaches to measuring curvature by developing a method that is explicitly linked to a particular model for network formation, the latent distance model of Hoff et al. (2002). Defining curvature based on a specific probabilistic model yields a direct connection between curvature and the underlying properties of a generative model for the graph. Specifically, we develop a consistent and asymptotically normal estimator of local curvature of the latent distance model. We also demonstrate that this estimator provides valuable insights when used in a number of existing statistical problems for network data. Specifically, we develop a hypothesis testing framework to reveal areas of non-constant curvature, which correspond to notions of brokerage in the sociology literature (Burt, 1992; Buskens and Van de Rijt, 2008). We also demonstrate that our estimator can be used in changepoint detection with an application to cybersecurity.

Moving now to discuss the probabilistic framework in more detail, the latent distance model consists of locations  $Z_i, Z_j$ , most generally on some metric space,  $\mathfrak{M}$ , often taken to be a smooth Riemannian manifold  $\mathcal{M}^p$  where the probability of forming an edge  $(i, j) \in E$  is inversely proportional to the distance on the latent manifold

$$g\left(P\left((i, j) \in E\right)\right) \propto -d_{\mathcal{M}}(Z_i, Z_j)$$

where  $g(\cdot)$  is some link function. The latent distance models and their extensions have been for such problems as modelling social influence (Sweet and Adhikari, 2020), social media relationships of politicians (Lok et al., 2021) and neuron connectivity (Aliverti and Durante, 2019) among numerous others.

The true latent geometry has implications on the global network properties. For example, spherical (positively curved) spaces form triangles and clusters more often than flat spaces and hyperbolic (negatively curved) spaces tend to generate tree-like structures (Smith et al., 2017). In other generative models of networks, the degree distribution and clustering of the network have implications of epidemic severity in network based SIR models (Volz et al., 2011), suggesting links to further properties of interest among network data.

Lubold et al. (2020) constructed a method of identifying the latent curvature. However, this generally required first picking a sign of the curvature prior to estimation, relies on global constant curvature and does not exhibit reliable asymptotics. One study of discrete graph curvature from the physics literature illustrates consistency to a global manifold in a special case (van der Hoorn et al., 2020). The authors study the convergence of a modified Ollivier-Ricci curvature, to the Ricci curvature of the underlying space in random geometric graphs under the limit of the connection radius shrinking to 0. Smith et al. (2017) also provide a method for identifying curvature based on simulations which compare the eigenspectrum of the graph Laplacian to models under spherical, hyperbolic and Euclidean geometry.

The remainder of the paper continues as follows. First, in Section 2 we introduce the statistical model as well as manifolds of constant curvature and necessary background geometry. We then introduce the curvature equation which allows for the identification of distances given the knowledge of a midpoint. We follow up with asymptotic theory for a known midpoint. We then establish convergence rates for midpoint set formation. In Section 4 we consider the practical methods for estimation, and discuss downstream statistical

tasks as well as include simulations under a mixture model. Next, we discuss downstream statistical tasks in such as a test of constant curvature in Section 5 and detecting change-points in Section 6. We further elaborate on these with applications of these methods to co-authorship networks in physics as well as an application in cybersecurity.

## 2 Methods

We will begin with an introduction of the models under consideration, then follow up with an introduction of the estimator and the associated asymptotic theory. We follow this up with a discussion of the bias associated with a point that is not exactly the midpoint of two other points and discuss the rate of convergence of the best approximation to a midpoint of two other points. Lastly we discuss estimation of distance matrices in the generative network model.

### 2.1 Generative Model

We consider the random symmetric network corresponding to a graph  $G = (V, E)$  where  $|V| = n$ , with adjacency matrix  $A \in \{0, 1\}^{n \times n}$  such that  $A_{ij} = 1$  iff  $(i, j) \in E$ . We suppose that this random adjacency matrix is generated under a latent distance model (Hoff et al., 2002) with random effects.

$$P(A_{ij} = 1 | \nu, Z) = \exp\left(\nu_i + \nu_j - d_{\mathcal{M}}(Z_i, Z_j)\right) \quad (1)$$

where

$$Z_i \sim_{iid} F_Z$$

$$\nu_i \sim_{iid} F_\nu$$

with random effect measure ( $F_\nu$ ) with support on the non-positive real line  $\text{supp}(F_\nu) \subset (\infty, 0]$  and where *iid* refers to sampling identically and independently from the latent distribution. This model relates the latent distances of the generative model to the probability of a connection between two points. Though not discussed in this paper, simple generalizations can be derived for directed networks. The latent position measure ( $F_Z$ ) has support on some unknown latent manifold  $\mathcal{M}^p$  (of dimension  $p$ ). The task of this paper is to estimate the curvature of  $\mathcal{M}^p$ . The  $\exp(\cdot)$  link function is used as an example for ease of explanation, however in the appendix we discuss the extension to the  $\text{expit}(\cdot)$  model as well as possible further extensions.

Latent distance models *typically* assume a class of simply connected Riemannian manifolds of constant sectional curvature ( $\kappa$ ), classically, the Euclidean  $\mathbb{E}^p$ , ( $\kappa = 0$ ) and spherical  $\mathbb{S}^p(\kappa)$ , ( $\kappa > 0$ ) and more recently the hyperbolic space  $\mathbb{H}^p(\kappa)$  ( $\kappa < 0$ ). However there are some extensions which are not restricted to this structure (Fosdick et al., 2016; Lok et al., 2021). By the Killing-Hopf theorem (Killing, 1891), these are the only manifolds of constant sectional curvature. We will refer to these latent spaces as the **canonical manifolds**. These are selected for two reasons. Firstly there are techniques for visualization for each of these methods (for  $p = 2$ ), thus highlighting the roles of individuals in the estimated model, and secondly, closed form expressions are available for the distances, allowing for estimation of these models. Embedding latent positions in a general Riemannian manifold would require the solving numerous variational optimization problems (computing geodesics/distances), preventing their use in practice. For a broader introduction on Riemannian geometry see Klingenberg (1995).

## 2.2 Models of Canonical Manifolds

Each of these canonical manifolds can be represented using a set of positions with real valued vectors and a corresponding distance function. We include definitions for Euclidean, spherical, and hyperbolic spaces for completeness.

The Euclidean manifold will be equipped with the standard  $\ell_2$  norm  $\mathbb{E}^p$  which describes the set of points for which  $x, y \in \mathbb{R}^p$  with distance matrix

$$d_{\mathbb{E}^p}(x, y) = \sqrt{\sum_{k=1}^p (x_k - y_k)^2}$$

The spherical model with curvature  $\kappa > 0$  is equivalent to the sphere of radius  $r = \frac{1}{\kappa^2}$ .

A simple way of expressing this is via the following model. A set of points are embedded in  $\mathbb{S}^p$  if  $x \in \mathbb{R}^{p+1}$ ,  $\sum_{k=0}^p x_k^2 = 1$ . We add a zero indexed coordinate for the spherical and hyperbolic models. We compute a signature  $B_{\mathbb{S}^p}$  and distances are computed via the signature

$$B_{\mathbb{S}^p}(x, y) = \sum_{k=0}^p x_k y_k$$

$$d_{\mathbb{S}^p}(x, y) = \frac{1}{\sqrt{\kappa}} \arccos(B_{\mathbb{S}^p}(x, y))$$

The hyperboloid model with curvature  $\kappa < 0$  corresponds to a set of points in  $\mathbb{H}^p$  if  $x \in \mathbb{R}^{p+1}$ ,  $x_0^2 - \sum_{k=1}^p x_k^2 = 1, x_0 > 0$ . An analogous signature  $B_{\mathbb{H}^p}$  exists for the hyperbolic embedding.

$$B_{\mathbb{H}^p}(x, y) = x_0 y_0 - \sum_{k=1}^p x_k y_k$$

$$d_{\mathbb{H}^p}(x, y) = \frac{1}{\sqrt{-\kappa}} \operatorname{acosh}(B_{\mathbb{H}^p}(x, y))$$

In our setting we do not require  $\mathcal{M}^p$  to have constant curvature, but we do make some much more mild assumptions on  $\mathcal{M}^p$ . We consider  $\mathfrak{M} = (\mathcal{M}^p, d)$  the metric space induced by the Riemannian manifold.

- (A1) (**Algebraic Midpoint Property**)  $\mathfrak{M}$  satisfies the algebraic midpoint property. For any  $x, y \in \mathcal{M}^p$  there exists a point  $z$  such that  $d_{\mathcal{M}^p}(z, x) = d_{\mathcal{M}^p}(z, y) = \frac{1}{2}d_{\mathcal{M}^p}(y, x)$ .
- (A2) (**Locally Euclidean**) For all  $p \in \mathcal{M}^p$  there exists some  $\delta > 0$  and some  $c_p, C_p$  such that for all  $\epsilon \leq \delta$ :

$$c_p(\delta) \leq \frac{\text{Vol}(B_{\mathcal{M}^p}(\epsilon, q))}{\text{Vol}(B_{\mathbb{R}^p}(\epsilon, 0))} \leq C_p(\delta)$$

and

$$\lim_{\epsilon \rightarrow 0} \frac{\text{Vol}(B_{\mathcal{M}^p}(\epsilon, q))}{\text{Vol}(B_{\mathbb{R}^p}(\epsilon, 0))} = 1$$

where  $B_{\mathcal{M}^p}(\epsilon, q)$  is the  $\epsilon$  ball on  $\mathcal{M}^p$  centred at a point  $q$ . Unless otherwise specified, from here if denoting  $B(\epsilon, q)$  we are referring to the ball on the latent manifold  $\mathcal{M}^p$ .

If  $\mathcal{M}^p$  is a connected manifold with scalar curvature upper and lower bounded, then these properties are satisfied. See Section E in the appendix for details.

## 2.3 Curvature and Estimating Equation

A number of methods exist to verify whether a particular set of distances can be embedded in a space of constant curvature. These include Schoenberg (1935) and Begelfor and Werman (2005) as well as Cayley-Menger determinants (Blumenthal and Gillam, 1943). Lubold et al. (2020) previously used these methods in order identify whether a set of dis-

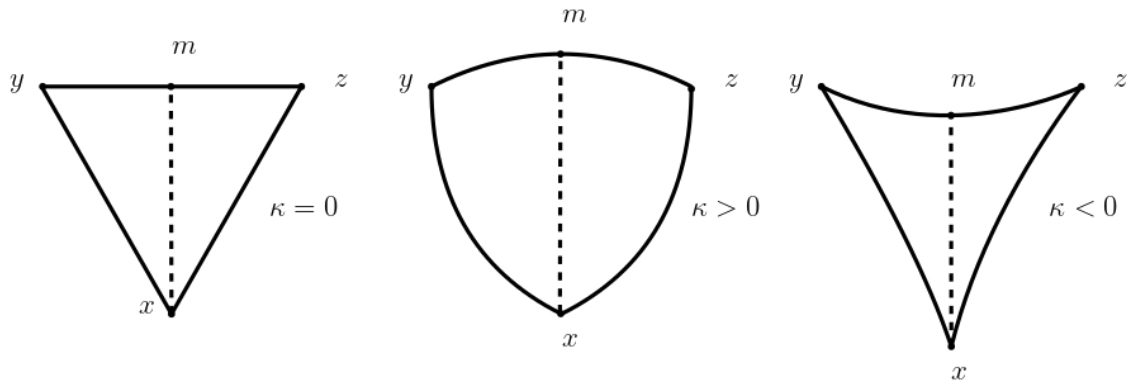


Figure 1: Midpoint distances and curvature of the space. The distance  $d_{xm}$  is an increasing function of the curvature  $\kappa$  for fixed other triangle side lengths

tances could be globally embedded in a particular curvature space. In this work, we take a different approach where we can identify curvature based on a minimal set of points.

We rely on a simple geometric insight. Consider a set of three points that form a triangle. If we look at the midpoint of any of the sides of this triangle, we can construct a distance from the midpoint to the opposite vertex. This length reveals the sectional curvature of the manifold, where a smaller distance corresponds to a more negatively curved space and a larger distance corresponding to a more positively curved space. This is visualized in Figure 1 for Euclidean, spherical and hyperbolic triangles.

This use of midpoints will help us identify the curvature of the latent space. For example, consider a case where no midpoint is present in the data. We let 4 points placed equidistant from each other, we can either embed these in  $\mathbb{E}^3$  or  $\mathbb{S}^2(\kappa)$  for  $\kappa > 0$ . Therefore the curvature of the latent space cannot be identified from this configuration. Though conditions like Schoenberg's, (Schoenberg, 1935) which are used in Lubold et al. (2020) can determine whether a distance matrix can be embedded in a space of constant curvature, identifiability concerns remain.

We instead take a much more direct approach at eliciting curvature, through the use of the existence of a midpoint. This lets us identify a curvature with only 4 points in total. The use of a midpoint allows us to work with a sub-manifold of dimension 2 which as long as  $p \geq 2$  will allow for identification of the curvature, circumventing the need to identify the dimensionality of the latent space. We will introduce an estimator for the curvature of the latent space and derive its asymptotic distribution in the case of a known midpoint. We follow this up with a discussion regarding the convergence rate of surrogate (approximate) midpoints.

We now formalize this intuition. For any 3 points  $x, y, z$  which lie in an unknown Riemannian manifold of dimension  $p \geq 2$  of constant sectional curvature  $\kappa$ ,  $(x, y, z)$  can be isometrically embedded in a sub-manifold of dimension 2.

**Definition 2.1.** *A submanifold  $\widetilde{\mathcal{M}} \subset \mathcal{M}$  is totally geodesic if every geodesic in  $\widetilde{\mathcal{M}}$  is also a geodesic in  $\mathcal{M}$ .*

We will use the fact that a totally geodesic submanifold contains all points along the geodesic, including the midpoint.

**Lemma 2.2.** *For any  $x, y, z \in \mathcal{M}^p(\kappa)$  if  $m$  is a midpoint lying between  $y$  and  $z$ . Then  $x, y, z, m \in \mathcal{M}^2(\kappa)$  where  $\mathcal{M}^2(\kappa)$  is a totally geodesic submanifold of dimension 2.*

The proof is straightforward and in Section A.1. The main implication here is that the totally geodesic submanifold allows us to look at distances in a subspace of dimension 2 which allow for identification. The three points  $x, y, z$  will fall into one of these submanifolds,  $m$  which lies on the geodesic between  $y$  and  $z$ . Since geodesics determine the distance, and geodesics on the submanifold are the same as geodesics on the total manifold, then this gives a criteria for identifying the latent curvature through the fortunate alignment of midpoints.

We now use this fact to derive an equation which will relate the curvature  $\kappa$  to the set of distances between the points  $(x, y, z, m)$ .

**Theorem 2.3** (Midpoint Curvature Equation). *Suppose that points  $x, y, z \in \mathcal{M}^p(\kappa)$  an unknown Riemannian manifold of dimension  $p$  of constant sectional curvature  $\kappa$ . Let  $m$  denote the midpoint between  $y, z$ . The following equation holds for  $\kappa \in \mathbb{R}$ .*

$$g(\kappa, d) = \operatorname{Re} \left[ \frac{2 \cos(d_{xm} \sqrt{\kappa}) - \sec\left(\frac{d_{yz}}{2} \sqrt{\kappa}\right) (\cos(d_{xy} \sqrt{\kappa}) + \cos(d_{xz} \sqrt{\kappa}))}{\kappa} \right] = 0 \quad (2)$$

Where  $d_{jk}$  denoted the distance between points  $j, k$  and  $\operatorname{Re}[\ ]$  denotes the real part of the equation.

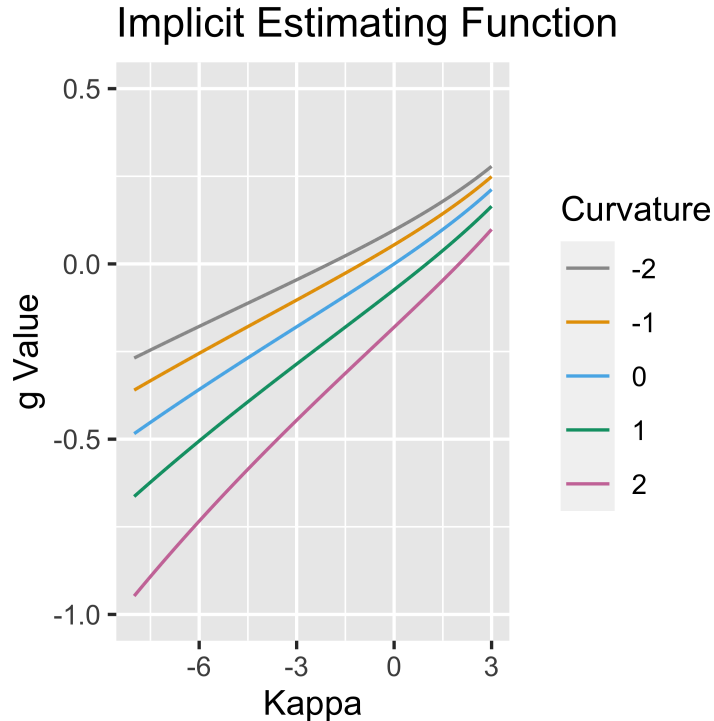
For cases when  $\kappa < 0$ , we take the real part of the above equation, which is equivalent to

$$g(\kappa, d) = \frac{2 \cosh(d_{xm} \sqrt{-\kappa}) - \operatorname{sech}\left(\frac{d_{yz}}{2} \sqrt{-\kappa}\right) (\cosh(d_{xy} \sqrt{-\kappa}) + \cosh(d_{xz} \sqrt{-\kappa}))}{\kappa}$$

The proof is found in the appendix in Section A.2. In essence, this equation is related to Toponogov's theorem (Klingenberg (1995) 2.7.12), which can be used to define a parameter based on distances  $\theta_T$  based on distances of a triangle  $x, y, z$ .

$$\theta_T(d) := \frac{1}{2}d^2(x, z) + \frac{1}{2}d^2(x, y) + \frac{1}{4}d^2(y, z) - d^2(x, m).$$

If the sectional curvature of  $\mathcal{M}^p$  is non-negative, then  $\theta_T(d) \geq 0$  and if the curvature is non-positive  $\theta_T(d) \leq 0$ . In Euclidean space, this reduces to the parallelogram law. Toponogov's theorem itself does not identify curvature, but if we assume that the points  $x, y, z, m \in \mathcal{M}^2(\kappa) \subseteq \mathcal{M}^p$  a totally geodesic submanifold of dimension 2 which is simply connected and of constant curvature, then this set of distances can be used to identify the curvature. The important distinction between this method of identification via Schoenberg (1935) or through Cayley-Menger determinants (Blumenthal and Gillam, 1943) is



as

Figure 2: Example of estimating functions  $g$  as a function of  $\kappa$ .

that these do not include the information of a midpoint whereas ours does. Additionally, these embedding theorems do not necessarily allow for the unique identification of curvature, but rather if a particular space of constant curvature can embed a given distance matrix.

To highlight the smoothness of our estimating function we plot a set of examples. For a unit equilateral triangle, we compute the corresponding midpoint distance  $d_{xm}$  for each curvature space with  $\kappa \in \{-2, -1, 0, 1, 2\}$ . We see in Figure 2 that our proposed estimating equation is differentiable around the solution with non-zero derivative, allowing one to identify the curvature from the  $\kappa : g(\kappa, d) = 0$ .

## 2.4 Curvature Estimation

Now that we have an estimating function which allows us to identify curvature, we discuss the estimator's asymptotics.

**Theorem 2.4.** *Suppose we have points  $x, y, z$  with midpoint the midpoint of  $y$  and  $z$  denote  $m$  on  $\mathcal{M}^p(\kappa)$ . Let  $\hat{d} = (\hat{d}_{xy}, \hat{d}_{xz}, \hat{d}_{yz}, \hat{d}_{xm})$  be the estimated distances and  $d = (d_{xy}, d_{xz}, d_{yz}, d_{xm})$  be their true, unknown counterparts. Assume*

- (B1) *We have a distance estimator such that  $\sqrt{r(n)}(\hat{d} - d) \rightarrow N(0, \Sigma)$*
- (B2)  $\kappa < \left( \frac{\pi}{\max\{d_{xy}, d_{xz}, d_{yz}, d_{xm}\}} \right)^2$
- (B3)  $\left| \frac{\partial g(\kappa, d)}{\partial \kappa} \right| > 0$

Where  $r(n)$  is the rate of convergence. Let  $\hat{\kappa}$  to the solution to of  $g(\kappa, \hat{d}) = 0$ . Then

$$\sqrt{r(n)}(\hat{\kappa} - \kappa) \rightarrow_d N \left( 0, \left( \frac{\partial g(\kappa, d)}{\partial \kappa} \right)^{-2} (\nabla_d g(\kappa, d))^T \Sigma \nabla_d g(\kappa, d) \right) \quad (3)$$

where  $\rightarrow_d$  refers to convergence in distribution.

The proof is found in the appendix in Section A.3 and is an application of the implicit function theorem and the delta method. In the proof, we also discuss the reasonableness of assumption (B3), which corresponds to the uniqueness of the root of the estimating function in the using the true distances, with an example taken from the Euclidean case. The implications here are that if we have an asymptotically normal distance estimate, then the estimate for the curvature will also be asymptotically normal. In our applications we will find that  $r(n) = \ell^2$ , where  $\ell$  is the size of the cliques used to construct the distance matrix. However if one has distance estimates at a faster rate, then these can be plugged in to obtain faster curvature estimates. Of course, this requires the knowledge of a true midpoint

as well. In the following sections, we discuss the use of approximate midpoints, as well as introduce techniques for estimating the distances on the underlying manifold.

## 2.5 Midpoint Bias

Until this point we have worked under the assumption that there is a known midpoint for a particular pair of points. However, in general, this is not known. Suppose that  $m'$  is a point which is a *surrogate midpoint* ( $m'$ ) for the midpoint between  $y, z$  and we have the analogous distance  $d_{xm'}$ . By a Taylor series expansion:

$$\begin{aligned}
0 &= g(\kappa', d') - g(\kappa, d) \\
&= \nabla_{\kappa} g(\kappa, d)(\kappa - \kappa') + \nabla_{d_{xm}} g(\kappa, d)(d_{xm} - d_{xm'}) + o(|\kappa - \kappa'|) + o(|d_{xm} - d_{xm'}|) \\
\implies |\kappa - \kappa'| &\approx (\nabla_{\kappa} g(\kappa, d))^{-1} \nabla_{d_{xm}} g(\kappa, d) |d_{xm} - d_{xm'}| \\
&\leq (\nabla_{\kappa} g(\kappa, d))^{-1} \nabla_{d_{xm}} g(\kappa, d) d_{mm'}
\end{aligned}$$

Hence, we can bound the approximation error for any fixed  $d, \kappa$  linearly in the distance between the true midpoint  $m$  and the surrogate midpoint  $m'$ . The surrogate midpoint does not satisfy the algebraic midpoint property exactly, but will be close. We next provide an outline involving how fast we can expect surrogate midpoints form.

Suppose that  $K$  points are sampled on a latent manifold  $\mathcal{M}^p$  of dimension  $p$  according to a continuous measure  $F_Z$ .

**Theorem 2.5.** *Suppose that  $Z_i \stackrel{iid}{\sim} F_Z$  are  $K$  points sampled iid from an unknown latent distribution on a simply connected manifold  $\mathcal{M}^p$ . Denote this set of points  $\{Z_i\}_{i=1}^K = \mathcal{D}_K$ . Suppose there exists a convex region  $A$  for which*

- (C1)  $f(z) \geq \alpha > 0$ , for all  $z \in A$

- (C2)  $\dim(A) = p \geq 2$

for all  $z \in A$  where  $f$  is the density function corresponding to  $F_Z$ . Further assume that

$$\max\{P[d(m(Z_i, Z_j), m(Z_k, Z_l)) \leq t], P[d(m(Z_i, Z_j), m(Z_j, Z_l)) \leq t]\} \leq C_p t^p \quad (4)$$

Define the statistic

$$\Phi(\mathcal{D}_K) := \min_{x, y, z \in \mathcal{D}: x \neq y, x \neq z, y \neq z} d\left(m(y, z), x\right)$$

Then

$$\Phi(\mathcal{D}_K) = \mathcal{O}_P(K^{-3/p}) \quad (5)$$

Our approach to showing the above result draws on similarities to Cai et al. (2013); Brauchart et al. (2015) which discuss convergence of the minimum distance between any two points sampled uniformly on a hypersphere. The authors show that  $\min_{i,j} d(Z_i, Z_j) = \mathcal{O}_P(K^{-2/p})$ , though they also derive an exact distribution for  $\min_{i,j} d(Z_i, Z_j)$  using the extra assumption of uniformity on the sphere. The authors use a technique by recursively computing the probability that a point is at least a radius  $\epsilon$  away from from the previous  $K$  points. Since at each placement of a new point, there are  $\binom{K}{2}$  midpoints as opposed to  $K$  current points, leading to the faster rate we observe.

The assumption in equation (4) is relatively mild as long as we do not consider point masses, but will not be problematic for continuous densities.

The proof is left to the Section A.8 in the appendix but relies on the following Theorem regarding medians of arbitrarily correlated random variables which may be of independent interest.

**Theorem 2.6.** *Consider a set of continuous random variables  $X_i$  which are marginally identical but have an arbitrary dependency. Let  $\widehat{\mathbb{M}}[X]$  denote the sample median of the set*

of these random variables. Then

$$P(\widehat{\mathbb{M}}[X] \leq t) \leq 2P(X \leq t) \tag{6}$$

We find the proof in in the appendix in Section A.7. Note that this bound is only useful up to  $t = \mathbb{M}[X]$  at which point the upper bound is 1. The implication here is that we only need most of the midpoints between any two points to be reasonably separated. We later illustrate how we will find good midpoints and so we can verify their existence in any observed dataset.

### 3 Distance Matrix Estimation

Previously we have not assumed that we have network distances, but a general distance matrix. In this section we introduce a method for estimating a distance matrix under the latent distance model. If we knew the curvature of the manifold, we could use maximum likelihood or other statistical techniques to estimate latent positions and, therefore the latent distances. This approach is commonly used in practice when the manifold geometry is assumed *a priori*. In our case, however the goal is to estimate the underlying curvature, so we need a notion of distance that is consistent across geometries.

We exploit a similar strategy to Lubold et al. (2020) in constructing a distance matrix. Specifically, we construct distances using connections across cliques, or fully connected subgraphs. This approach has two advantages. First, since cliques represent multiple nodes we have multiple opportunities for there to be connections between two cliques, meaning we can use the fraction of realized ties between two cliques as an estimate for the probability of connection between the two cliques. Since our approach relies on a specific probability model for connections, we can easily convert connection probabilities into distances us-

ing the parametric model. Second, in general, cliques will correspond to points near each other in space. This means that we can consider cliques as “points” on the manifold that can be used to identify a distance matrix.

We now proceed to describe our approach in detail. In order to estimate the distance matrix, we first assume we have access to the person-specific effects and focus only on the distances. We later relax this as it will be negligible if we can estimate them at a fast enough rate. Under this model, we assume nodes of a clique have nearly the same latent distance. Let  $X, Y \in \{1, 2, \dots, n\}$  denote sets of nodes which denote non-overlapping cliques. Then the average probability of connection can be used to identify the latent distance, if we can also estimate the average of random effects ( $\nu$ ). Let  $|W|$  denote the size of  $W \in \{X, Y\}$ . We define the average probability of connection across cliques  $X, Y$  as the following.

$$\begin{aligned}
p_{XY} &:= \frac{1}{|X||Y|} \sum_{x \in X} \sum_{y \in Y} p_{xy} \\
&= \frac{1}{|X||Y|} \sum_{x \in X} \sum_{y \in Y} \exp(\nu_x + \nu_y - d(x, y)) \\
&= \exp(-d(x, y)) \frac{1}{|X||Y|} \sum_{x \in X} \sum_{y \in Y} \exp(\nu_x + \nu_y) \\
\implies d(x, y) &= -\log(p_{XY}) + \log\left(\frac{1}{|X|} \sum_{x \in X} \exp(\nu_x)\right) + \log\left(\frac{1}{|Y|} \sum_{y \in Y} \exp(\nu_y)\right) \\
&= -\log(p_{XY}) + \gamma_X + \gamma_Y \\
\gamma_W &:= \log\left(\frac{1}{|W|} \sum_{w \in W} \exp(\nu_w)\right) \quad \text{for } W \in \{X, Y\}
\end{aligned}$$

Since there are  $\ell^2$  possible connections between a pair of cliques of size  $\ell$ , we can construct an asymptotically normal estimator of  $p_{XY}$  by just the plug in sample average of connections. However, in order for these asymptotics to hold, we must estimate  $\gamma_X$  and  $\gamma_Y$  at rates  $o_P(\frac{1}{\ell})$ , so that these are asymptotically negligible nuisance parameters. A final issue that remains however is the restriction of all distance estimates to ensure that they pre-

serve a metric structure. We will illustrate our solutions to these problems in the following sections.

Unless latent positions are nearly (or exactly) in the same location, large cliques are rare in latent space models. The next lemma illustrates a rate of convergence of these latent locations relative to the size of a clique.

**Lemma 3.1.** *Assume the latent distance model as in equation (1)  $\Delta_\ell = \max_{i,j} d(Z_i, Z_j)$  and let  $C_\ell$  denote the event that nodes  $i = 1, \dots, \ell$  form a clique. If*

- (D1) *For some  $\delta > 0$  there exists  $c_2$  such that for all  $\epsilon < \delta$ ,  $\sup_{q \in \mathcal{M}^p} F_Z(B(\epsilon, q)) \geq c_2 \epsilon^p$*

*Let  $\mu_d = \mathbb{E}[d(Z_i, Z_j)]$  where  $Z_i$  and  $Z_j$  are drawn independently from  $F_Z$ . Then for any  $0 < \tilde{\mu}_d < \mu_d$*

$$\Delta_\ell | C_\ell = o_P(\exp(-\tilde{\mu}_d \ell)).$$

*for all  $\epsilon > 0$ . I.e. conditionally on the existence of a clique, the locations of the latent positions converge at an exponential rate.*

See the appendix Section A.4 for a proof. The main implication is that it is reasonable to treat the latent positions as a single point when nodes are within a clique. The assumption in Lemma 3.1 ensures that we have some region in the latent space where positions can be drawn near each other, if there is a point mass anywhere on the latent space, then this condition is immediately satisfied, otherwise, if  $F_Z$  admits a smooth continuous density ( $f_z$ ) then it is also satisfied in any region of positive density value, since  $\mathcal{M}^p$  satisfies the locally Euclidean property (A2).

In order to estimate  $d_{xy}$  we must estimate the nuisance parameters  $\gamma_X$  and  $\gamma_Y$  at a fast

enough rate. If a set of nodes are generated from a common point, as in a clique, we can use the number of connections a point has to the rest of the network in order to identify the relative difference in their random effects. We assume that all points within a clique share the same latent position. We show in Lemma 3.1 that this assumption is reasonable as the latent radius of the points shrinks exponentially fast. Consider a set of nodes  $i \in X$  where  $X$  denotes the indices of a clique. Let  $k$  denote the indices of any other node in the network. Then we can identify the differences of random effect values within a clique

$$\begin{aligned} P(A_{ik} = 1) &= \int \exp(\nu_i + \nu_k + d(z_i, z_k)) dF_Z(z_k) dF_\nu(\nu_k) \\ &= \exp(\nu_i) \int \exp(\nu_k + d(z_i, z_k)) dF_Z(z_k) dF_\nu(\nu_k) \\ \implies \frac{P(A_{ik} = 1)}{P(A_{jk} = 1)} &= \exp(\nu_i - \nu_j). \end{aligned}$$

Other than in pathological cases,  $\ell \ll n$  where  $n$  is number of nodes in the network. As a result, we are able to measure the differences between the random effects of members of a clique quite effectively, at a rate of  $O_P(\frac{1}{\sqrt{n}})$ . Therefore, we can define  $\nu_i = \nu_X + \Delta\nu_i$  which allows us to identify  $\Delta\nu_i$  if  $\nu_X = \min_{i \in X} \nu_i$  were known,

$$\gamma_X = \nu_X + \log \left( \frac{1}{|X|} \sum_{i \in X} \exp(\Delta\nu_i) \right).$$

The remaining question is to estimate  $\nu_X$ . We will argue that the smallest random effect under mild conditions will converge to 0 at an exponentially fast rate.

**Lemma 3.2.** *Let  $C_\ell$  denote the event that  $i \in \{1, 2, \dots, \ell\}$  form a clique. Suppose that*

1. (E1) *For some  $\tilde{\delta} > 0$  for all  $0 < \delta < \tilde{\delta}$ ,  $F_\nu(\nu_i > -\delta) \geq c_3 \delta$*

Let  $\mu_\nu := E[\nu]$  Then for any  $\mu_\nu < \tilde{\mu}_\nu < 0$

$$\min_i \nu_i | C_\ell = o_P(\exp((\tilde{\mu}_\nu)\ell)) \quad (7)$$

This theorem states that the nodes which we find in a clique, tend to have near 0 random effects, and thus it is reasonable to set  $\max_i \nu_i = 0$  in an estimator. Note that this is an exponential rate which can be arbitrarily close to  $(\exp(\mu_\nu \ell))$ .

**Lemma 3.3.** *Let  $W \subset \{1, 2, \dots, n\}$  denote a subset of indices which form a clique ( $C_\ell$ ). Let  $d_i$  denote the degree of node  $i \in W$  where  $|W| = \ell$  and assume that the points in the clique have a common latent position. Denote the estimator of  $\gamma_W$*

$$\hat{\gamma}_W = \log \left( \frac{1}{\ell} \sum_{i \in W} \frac{d_i}{\max_{j \in W} d_j} \right).$$

Then if (E1) in Lemma 3.2 holds, then define  $\tilde{\mu}_\nu$  as in Lemma 3.2

$$\hat{\gamma}_W - \gamma_W = \mathcal{O}_P \left( \max \left\{ \exp(\tilde{\mu}_\nu \ell), \frac{1}{\sqrt{n}} \right\} \right) \quad (8)$$

*Proof.* We note that conditional on the node of interest appearing in a clique  $\frac{d_i}{d_j} - \exp(\nu_i - \nu_j) = \mathcal{O}_P(n^{-1/2})$ . Then since  $\min_i \nu_i = \mathcal{O}_P(\exp(-\ell))$ . All of the random effects are converging to 0 and hence  $\min_i \nu_i = \mathcal{O}_P \left( \min \left\{ \exp(-\ell), \frac{1}{\sqrt{n}} \right\} \right)$ .  $\square$

Therefore, estimation of  $\gamma_W$  within a clique can occur at an exponential rate, meaning that this estimation will be negligible compared to the average cross-clique probabilities.

**Theorem 3.4.** *Let  $\hat{d}$  be a set of clique distances measured via connections between cliques of size  $\ell$ . Assume that we have indices of cliques  $X, Y$  for which  $|X| = |Y| = \ell$  and  $X \cap Y = \emptyset$ . We also assume the following nuisance estimators exist and that the Lederberg condition is satisfied for*

- (F1)  $\widehat{\gamma}_W - \gamma_W = o_P(\frac{1}{\ell})$  for  $W \in X, Y$
- (F2) **Lindeberg Condition**  $\lim_{\ell \rightarrow \infty} \frac{\sum_{x \in X} \sum_{y \in Y} (A_{xy} - p_{xy})^2 I(|A_{xy} - p_{xy}| > \epsilon \ell^2 \sigma_\ell)}{\sigma_\ell} = 0$  for all  $\epsilon > 0$

Where

$$p_{XY} = \frac{1}{\ell^2} \sum_{x \in X} \sum_{y \in Y} p_{xy} \quad (9)$$

$$\sigma_\ell = \frac{1}{\ell^2} \sum_{x \in X} \sum_{y \in Y} p_{xy} (1 - p_{xy}) \quad (10)$$

Then

$$\sqrt{\ell^2 \frac{\sigma_\ell}{p_{XY}}} \left( \widehat{d}(X, Y) - d(X, Y) \right) \rightarrow_d N(0, 1) \quad (11)$$

The proof is found in Section A.6. The main implication here is that if we can estimate the random effects fast enough within a clique, then we are able to estimate the random effects at a rate which is negligibly fast compared to the rate of  $\widehat{p}_{XY}$ . Additionally, we note that since in general, the random effects are all converging to 0 within a clique, that for large cliques  $p_{XY} \approx \exp(-d_{XY})$ , thus allowing for simplified expressions for  $\sigma_\ell$  and  $p_{XY}$ .

For a set of cliques  $\mathcal{C} : |\mathcal{C}| = K$ , we can compute a distance matrix  $\widehat{D} \in \mathbb{R}^{K \times K}$  such that we best fit the observed data while maintaining the restriction of the triangle inequalities. In this characterization and also in Lubold et al. (2020), the distance matrix estimation does not in fact necessarily respect the restrictions that all distance matrices must satisfy, namely non-negativity, and the triangle inequality. For example, we construct an enumeration of the cliques of size 7 or greater from the General Relativity co-authorship network of Leskovec et al. (2007) in Figure 3. Any pair of cliques which does not share an edge will inherently be estimated to have infinite distance, which prevents estimation of curvature. However applying the triangle inequality via other estimated distances in the graph would

allow us to construct an upper bound.

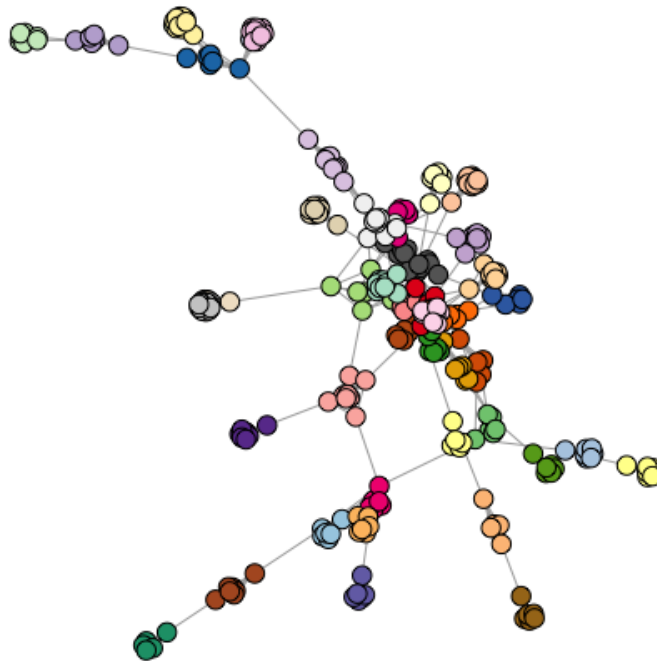


Figure 3: Clique subgraph of co-authorship network in ArXiv General Relativity. Cliques shown by color.

We can posit a similar estimation problem, while respecting the triangle inequality. The following estimation problem is posed below. Let  $X$  denote a set of indices corresponding to a single clique in a graph  $G$ . Let  $\mathcal{C}$  denote the set of cliques in an observed graph. Given a set of fixed effects, we can propose a maximum likelihood optimization problem for the distance matrix  $D \in \mathbb{R}^{K \times K}$  under the generative model. By the approximation that cliques have a common latent position, we define the following likelihood function of the

clique subset of the data  $\ell_{\mathcal{C}}$

$$\begin{aligned}\ell_{\mathcal{C}}(D; \boldsymbol{\nu}) &= \sum_{X,Y \in \mathcal{C}, i \in X, j \in Y} A_{ij} \log(P(A_{ij} = 1)) + (1 - A_{ij}) \log(P(A_{ij} = 0)) \\ &= \sum_{X,Y \in \mathcal{C}, i \in X, j \in Y} A_{ij} (\nu_i + \nu_j - D_{x,y}) + (1 - A_{ij}) \log(1 - \exp(\nu_i + \nu_j - D_{x,y})).\end{aligned}$$

Then we can define the maximum likelihood optimization problem, after estimating a set of random effects  $\hat{\boldsymbol{\nu}}$

$$\begin{aligned}\hat{D} &= \sup_{D \in \mathbb{R}^{K \times K}} \ell_{\mathcal{C}}(D; \hat{\boldsymbol{\nu}}) \\ \text{s.t. } &D_{x,y} \geq 0 \\ &\text{Diag}(D) = 0 \\ &\text{tr}(E_s^T D) \geq 0 \forall s \in \mathcal{S}\end{aligned}$$

where  $\mathcal{C}$  is a list of clique indices and  $E_s$  are matrices full of zeros other than 3 indices,  $i, j, k$  for which  $E[i, j] = E[i, k] = 1 = -E[j, k]$ . This set of indices allows us to respect the triangle inequality for all possible triplets of distances. We define  $\mathcal{S}$  to be an enumeration of all such indices  $E_s$ . There are  $3\binom{K}{3}$  such restrictions. The set of feasible distance matrices which satisfy these constraints form a polyhedron of interior dimension  $\binom{K}{2}$ . We see here that this becomes a convex problem under the space of symmetric matrices with many restrictions. In practice, we use `CVXR` to solve this system (Fu et al., 2020). For a greater gain in computational speed, we use the `MOSEK` solver in for the constrained optimization (Andersen and Andersen, 2000).

Though in its current form, the problem is numerically challenging to solve due to the number of restrictions. A natural option is to approximate the likelihood via a second order Taylor expansion and solve this problem successively. Since the Hessian is diagonal,  $\frac{\partial^2}{\partial d_{ij} \partial d_{kl}} \ell_{\mathcal{C}}(D; \boldsymbol{\nu}) = 0$  if  $d_{ij} \neq d_{kl}$ , this can be made into a more efficient quadratic program

which can be solved faster in CVXR.

Let  $g(D; D_0; \boldsymbol{\nu})$  be the second order Taylor series approximation to  $\ell_{\mathcal{C}}$  about a matrix  $D_0$

$$\begin{aligned}
\ell_{\mathcal{C}}(D; \boldsymbol{\nu}) &:= \sum_{X,Y \in \mathcal{C}, i \in X, j \in Y} A_{ij} (\nu_i + \nu_j - D_{x,y}) + (1 - A_{ij}) \log(1 - \exp(\nu_i + \nu_j - D_{x,y})) \\
&\approx \sum_{X,Y \in \mathcal{C}, i \in X, j \in Y} A_{ij} (\nu_i + \nu_j - D_{0,x,y}) + (1 - A_{ij}) \log(1 - \exp(\nu_i + \nu_j - D_{0,x,y})) \\
&+ \sum_{X,Y \in \mathcal{C}, i \in X, j \in Y} -A_{ij} (D_{x,y} - D_{0,x,y}) - (1 - A_{ij}) \frac{\exp(\nu_i + \nu_j - D_{0,x,y})}{1 - \exp(\nu_i + \nu_j - D_{0,x,y})} (D_{x,y} - D_{0,x,y}) \\
&+ \sum_{X,Y \in \mathcal{C}, i \in X, j \in Y} -(1 - A_{ij}) \frac{\exp(\nu_i + \nu_j - D_{0,x,y})}{(1 - \exp(\nu_i + \nu_j - D_{0,x,y}))^2} \frac{(D_{x,y} - D_{0,x,y})^2}{2} \\
&:= \tilde{g}(D, D_0; \boldsymbol{\nu})
\end{aligned}$$

And hence we can successively solve for  $\hat{D}_{t+1}$  the following constrained optimization problem

$$\begin{aligned}
\hat{D}_{t+1} &= \sup_{D \in \mathbb{R}^{K \times K}} \tilde{g}(D, \hat{D}_t; \hat{\boldsymbol{\nu}}) \\
&\text{s.t. } D_{x,y} \geq 0 \\
&\text{Diag}(D) = 0 \\
&\text{tr}(E_s^T D) \geq 0 \forall s \in \mathcal{S}
\end{aligned}$$

which can be iteratively computed until  $\ell_{\mathcal{C}}$  increases less than some threshold. Each iteration is a linear constrained quadratic program which we implement in CVXR. For further details, see the appendix in Section B.2.

## 4 Practical Considerations and Statistical Tests

In this section we consider some of the practical issues with estimation. In particular, how to choose a good midpoint, and how to filter points which we know to have extremely high variance. In general, we would like to find a set of points for which  $\widehat{d}_{ym} \approx \widehat{d}_{zm} \approx \frac{1}{2}\widehat{d}_{yz}$  with  $\widehat{d}_{yz}$  not excessively small.

### 4.1 Choosing Best Midpoint

In practice given a distance matrix we would like search over the space to find the best midpoint. For an unknown latent geometry, we can exploit the Fréchet mean of two points

$$m^* = \arg \min_{m \in \mathcal{M}} d^2(y, m) + d^2(z, m).$$

The midpoint between any two points  $y, z$  is also the Fréchet mean. Therefore we can search over the space of candidate entries of a distance matrix  $D$  to find the best midpoint available. In practice, we also would like to ensure that the points  $y, z$  are not too close to each-other. If  $y$  and  $z$  are too close to each-other, then this leads to a very high variance estimator. So a reasonable option is to normalize this quantity by  $d(y, z)$ . Given a true midpoint  $m^*$ , then  $d(y, m^*) = d(z, m^*) = \frac{1}{2}d(y, z)$ , then

$$\frac{d^2(y, m^*) + d^2(z, m^*)}{d^2(y, z)} = 1/2 \tag{12}$$

Therefore in order to compute the best surrogate midpoint set we solve the following prob-

lem

$$\hat{y}, \hat{z}, \hat{m} = \arg \min_{y, z, m} \frac{d^2(y, m) + d^2(z, m)}{d^2(y, z)} \quad (13)$$

## 4.2 Selecting Reference Points

Though all we need are 4 points in order to identify curvature, we are restricted by the fact that we have to find pairs with good surrogate midpoints. However, we will often observe many other potential locations which we can use for  $x$ . For example, it is very hard to elucidate curvature when  $x, y, z$  are nearly co-linear, and thus we would like triangles  $x, y, z$  which are closer to equilateral.

We exploit this by considering a scaled version of the triangle inequality. Let  $C_\Delta \in [1, 2]$  be a constant which determines the flatness of the allowed sets  $x, y, z$ . Then

$$d_{ij} + d_{jk} \geq C_\Delta d_{ik} \quad \forall (i, j, k) \in (x, y, z) \quad (14)$$

This tuning parameter allows us to pick the triangles closest to equilateral, which tend to give the best estimates of the curvature. Letting  $C_\Delta = 1$  allows for all triangles, no matter how flat they are and  $C_\Delta = 2$  will only permit exact equilateral triangles. In practice we find that a value of  $C_\Delta \in [1.2, 1.8]$  is effective and we set the default to be 1.4. Setting  $C_\Delta$  to be too large results in no triangles found, and setting  $C_\Delta$  too small will result in using triangles which are very flat, and often suffer from finite sample bias as well as high variance in their respective  $\hat{\kappa}$  estimates.

We can illustrate this phenomena using the theoretical gradients computed for the asymptotic results. We observe in Figure 4 that the smallest variance reference points in each of these curvatures are the ones which form nearly equilateral triangles with the reference points  $y, z$ .

Hence for a set  $(y^{(j)}, z^{(j)}, m^{(j)})$  we can compute a set of estimates  $\{\widehat{\kappa}^{(y^{(j)}, z^{(j)}, m^{(j)})}\}_{j=1}^J$  using all the  $x$  positions such that equation (14) is satisfied. If we wish to compute a single curvature estimate  $\widehat{\kappa}$  then a simple method will be to return the median over the set of estimates.

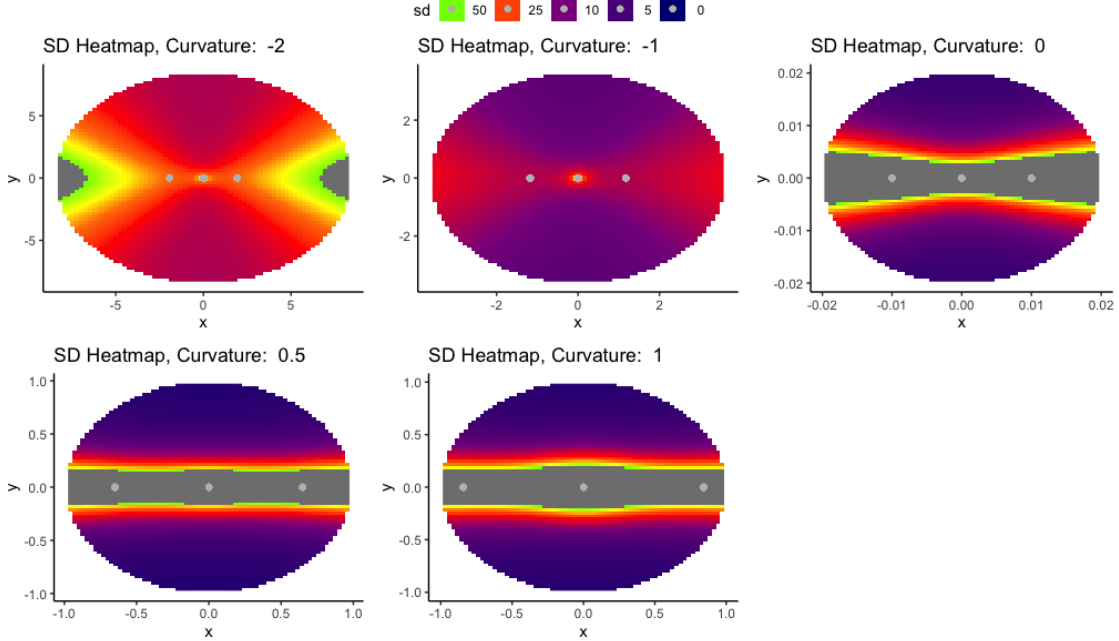


Figure 4: Variance as a function of  $x$  position. True points  $(y, m, z)$  in black.

### 4.3 Simulations

We construct a number of simulations in order to illustrate the consistent estimation of curvature. We see that in practice, generally we require relatively large cliques for accurate estimation. Additionally, many networks may have relative sparsity along with moderately large cliques. We note that in practice, the methods for finding maximal cliques are much faster under sparser graph conditions. We use the maximal clique finding function in `igraph` R package Csardi et al. (2006).

In order to simulate networks which preserve some of these properties, we sample from the

following model.

$$\begin{aligned}\mu_k &\sim F_{\mathcal{M}^p(\kappa)}^\mu(\mathbf{O}, R) \quad k \in \{1, \dots, \lceil \sqrt{\rho}50 \rceil\} \\ \sigma_k^2 &\sim F_{\sigma^2} \\ \boldsymbol{\pi} &\sim \text{Dirichlet}(\mathbf{2}) \\ \text{for } \kappa &\in \{-2, -1, -0.5, 0, 0.5, 1\} \\ \text{and } \rho &\in \left\{\frac{1}{\sqrt{2}}, 1, 2, 4\right\}\end{aligned}$$

where  $F_{\mathcal{M}^p(\kappa)}^\mu(\mathbf{O}, R)$  denotes the uniform distribution of radius  $R$  centred at the origin  $\mathbf{o}$  for  $\kappa \geq 0$  and for  $\kappa < 0$ , the latent distribution is sampled isotropic with radial density  $f(r) = \frac{2}{R}(R - r)I(r \leq R)$  with  $R = 2.5$ . The reasoning for this is that it allows for mid-points to form in the hyperbolic space. This process determines a random latent position cluster model (LPCM). The locations of  $\mu_k$  as well as the relative sizes of  $\sigma_k^2$  determine where cliques are most likely to form in the latent space.

We then sample a random adjacency matrix  $A$  via the sampled LPCM.

$$\begin{aligned}n &= 5000\rho \\ Z_i &\sim F_Z \\ \nu_i &\sim F_{\nu, \rho} \\ p_{ij} &= \exp(\nu_i + \nu_j - d(Z_i, Z_j)) \\ A_{ij} &\sim \text{Bern}(p_{ij})\end{aligned}$$

Where  $F_Z(\boldsymbol{\pi}, \boldsymbol{\sigma}^2, \boldsymbol{\mu})$  is a particular draw of the random latent position cluster model. And  $F_{\nu, \rho}$  is a trimmed normal distribution with mean  $-3\rho$  and standard deviation  $3\rho$  trimmed at 0 and  $\log(2/\sqrt{n})$  so that  $\nu_i$  remain non-negative and to prevent isolated nodes. We let the minimal clique size used in the estimator be of size  $\ell = (8 + 4\log(\rho))$ , which tend to

appear in quantities from 40 – 60 under this simulated dataset. For cliques smaller than 12 we use the maximal clique search algorithm implemented in `igraph` over the whole dataset, and for  $\ell = 16$  search over the subgraphs of node corresponding true cluster memberships to reduce the computational time. See Section F for additional graph statistics summaries over the simulations.

For the choice of latent space, we let  $\kappa \in \{-2, -1, -0.5, 0, 0.5, 1\}$  and  $p = 3$ . We illustrate that we can obtain a consistent estimator in Figure 5. We also illustrate the coverage of each of these test, highlighting that proper coverage is achieved as  $\ell$  increases in Figure 6 for  $C_\Delta = 1.8$ , however for  $C_\Delta = 1.6$  the negatively curved spaces may not have proper coverage at this level. This suggests a larger  $C_\Delta$  for proper coverage in negatively curved spaces.

## 5 Application: Constant Curvature Test

We consider a variant of the Kruskal-Wallis test (Kruskal and Wallis, 1952) which we will use for our tests of constant curvature. Given a set of random variables  $X_{ij}$  where  $i$  denotes the group,  $i \in \{1, 2, \dots, g\}$ . Let  $r_i$  denote the within group  $i$  average rank.

### Kruskal-Wallis Test:

1. Compute the ranks  $r_{ij}$  ignoring group membership,  $r_{ij} \in \{1, 2, \dots, N\}$
2. Compute the test statistic  $H := (N - 1) \frac{\sum_{i=1}^g n_i (\bar{r}_i - \bar{r})^2}{\sum_{i=1}^g \sum_{j=1}^{n_i} (r_{ij} - \bar{r})^2}$
3. Reject if  $H \geq H_{\alpha, g}$

where  $H_{\alpha, g}$  denotes a significance threshold. Exact distributions can be computed, however this distribution is asymptotically  $\chi_{g-1}^2$ .

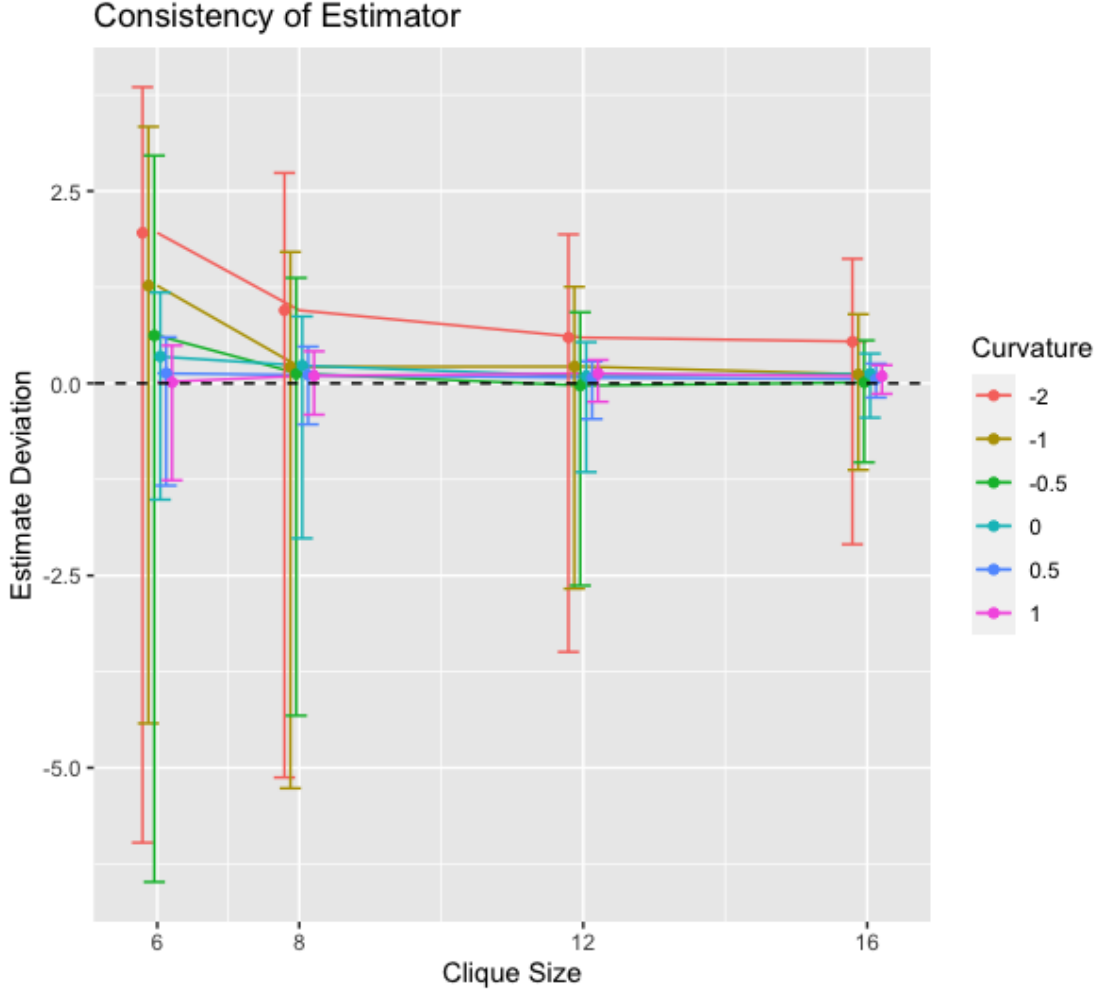


Figure 5: Consistency of Curvature Estimator

We can consider a similar test used for our setting. Let  $\{\widehat{\kappa}^{(r)}\}_{j=1}^{J_r}$  be a collection of estimates of curvature for which one wants to check whether there is a difference. This for example could be across views of a multiplex network, or it could be across regions in a single network using midpoint sets  $(y^{(r)}, z^{(r)}, m^{(r)})_{r=1}^R$ . We are interested in testing the hypothesis

$$H_0 : \kappa^r = \kappa \text{ for all } r \quad H_A : \kappa^{r'} \neq \kappa^r \text{ for some pair } r, r'.$$

Since the Kruskal Wallis test will detect a difference in distribution between the observa-

tions, we can transform and normalize the data in order to reduce the type 1 error rate due to outliers. We therefore introduce the preprocessed Kruskal-Wallis test.

**Preprocessed Kruskal-Wallis Test:**

For some  $c > 0$  (default  $c = 10$ )

1. Compute  $\tilde{y}^{(r,j)} = c \tanh(\hat{\kappa}^{(r,j)}/c)$
2. Re-normalize for each  $r$ ,  $\hat{y}^{(r,j)} = \frac{\tilde{y}^{(r,j)} - \text{med}_r\{\tilde{y}^{(r,j)}\}}{\text{mad}_r\{\tilde{y}^{(r,j)}\}} + \text{med}_r\{\tilde{y}^{(r,j)}\}$
3. Apply the Kruskal-Wallis test to test for differences in the distributions from the  $R$  samples  $\{\{\hat{y}^{(r,j)}\}_{j=1}^{J_r}\}_{r=1}^R$

Here  $\text{med}_r$  denotes the median indexed within a set  $r$  and  $\text{mad}_r$  is similarly the median absolute deviation. In finite samples, we find that for very negatively curved spaces, we have heavy negative tails, limiting our use of a simple ANOVA difference in means test. The preprocessing step tends to help match the general shape of the distributions such that the differences more likely correspond to differences in median. We find that this can be effective to give useful results in simulations.

**5.1 Simulations**

Under the same simulation setup as in Section 4.3 we can illustrate the coverage of the constant curvature test as a function clique size. We can also observe that for larger values of curvature, we tend to get type 1 error coverage faster, which is also similar to what is seen in Figure 5 in which the variance of the curvature estimate tends to be larger.

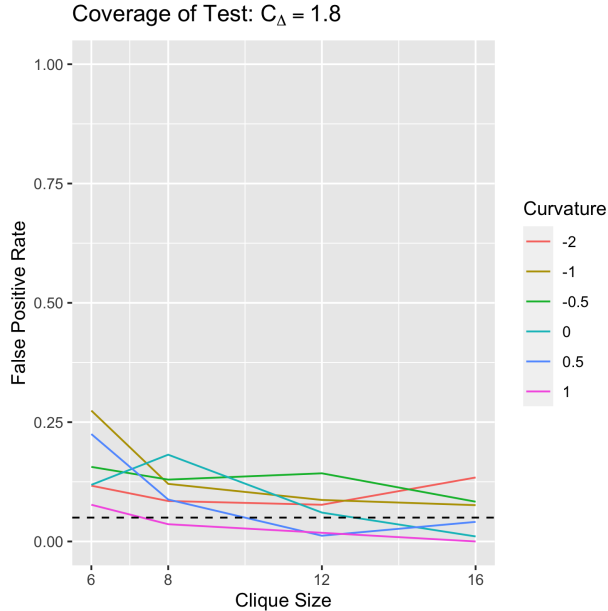


Figure 6: False positive rate for constant curvature test.

## 5.2 Multiplex Network Constant Curvature Tests.

In this first simulation, we consider a model of multiplex (or multiview) networks. Several methods exist for modelling multiplex networks via extensions of the latent distance model, however most assume the same geometry latent space among views Salter-Townshend and McCormick (2017); MacDonald et al. (2022). For example, Salter-Townshend and McCormick (2017) model the multiple relationships between individuals in the Banerjee et al. (2013) Indian villages dataset using Euclidean spaces. We illustrate an example where this is not the case.

We first construct a latent position model for which multiple views are drawn from a common set of latent positions, however, these positions are common coordinates of spheres of curvature  $(\kappa_1, \kappa_2) = (0.5, 1.5)$  respectively. Additional details for the simulation are identical to the consistency simulations in Section 4.3.

In this case for a set of latent positions, we simulate a multiplex network for which latent spherical positions are the same for this network set, however they are embedded in two

spheres of different radii and thus different curvature. We simulate 200 pairs of network and test the curvature difference and plot the power in Figure 7. In each view we compute the optimal midpoint set  $y^{(r)}, z^{(r)}, m^{(r)}$  from each view distance matrix  $\hat{D}^{(1)}$  or  $\hat{D}^{(2)}$  via equation 13 and use the preprocessed Kruskal-Wallis test to test for the difference in curvature between views.

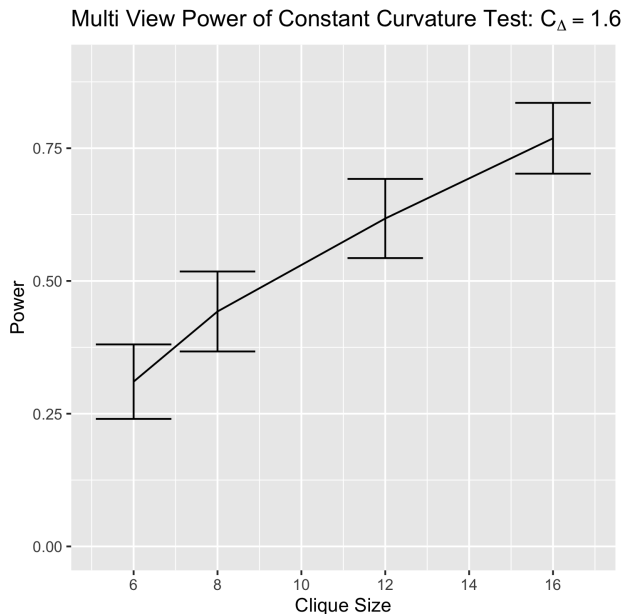


Figure 7: Power of constant curvature test across two views.

### 5.3 Noncanonical manifolds

We next illustrate the ability of our method to detect non-constant curvature within the latent space. Since many common latent space models are constantly curved, it is of interest to verify whether this agrees with the observed data.

Though the sphere, the hyperbolic and Euclidean spaces all have closed form solutions for their distances, this is not true of arbitrary manifolds, and we highlight our example on one which allows us to compute these distances.

We construct a latent space consisting of two adjacent spheres. For any two points in the same sphere the distance is straightforward to compute. For any two points  $(x, y)$  in opposite spheres, the distance can be computed via the distance to the origin  $(1, 0, 0)$  in each of the spheres. This is due to the fact any geodesic must pass through the connecting point, i.e. the origin.

$$d_{x,y} = d_1(x, o) + d_2(o, y)$$

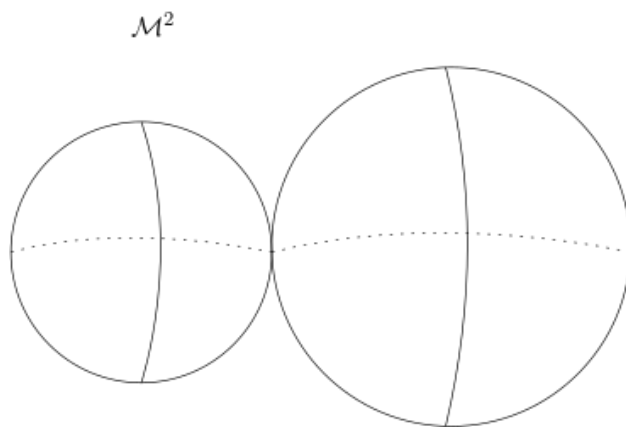


Figure 8: Adjacent spheres, a model of non-constant curvature.

For these simulations, our manifold consists of two adjacent spheres of curvature  $\kappa_1 = 1, \kappa_2 = 1.5$  respectively. This manifold was chosen as distances were straightforward to compute, but also does not contain a constant curvature. The latent cluster locations are sampled via uniforms centred on opposite poles. We again simulate 200 draws from the latent position cluster model and test for constant curvature by finding the best three non-overlapping sets minimizing equation (13). We plot the corresponding power in Figure 9.

## 5.4 Geometry of Coauthorship

We consider the sets of co-authorship networks introduced in Leskovec et al. (2007). These consist of citation networks from High Energy Particle Physics, General Relativity, Astro-

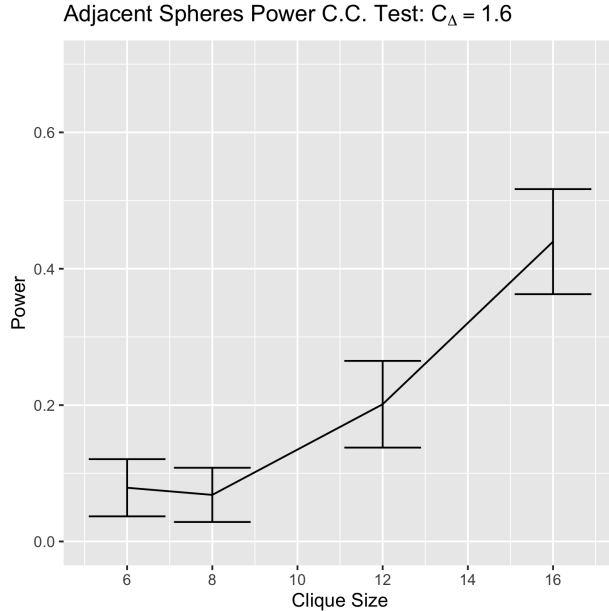


Figure 9: Constant Curvature Test Power: Adjacent Spheres

physics and Condensed Matter Physics, with sizes of each of the networks seen in Table 1. These networks consist of authors as nodes where an edge exists whether any pair of authors has co-authored a paper on ArXiv in any of the specified subject areas between 1993 and 2003. When these data were collected, these were the top 5 most common subject areas in Physics.

In previous ML applications, hyperbolic network embeddings have been successful in tasks such as link-prediction or node in citation networks (Nickel and Kiela, 2017; Chami et al., 2019; Chamberlain et al., 2017). This is due to the fact that the hierarchical structure (tree-like) structure generally can be more easily embedded in a negatively curved space. We wish to answer the question of, under a latent space assumption, is the data generated from a space of constant curvature?

For each of these networks we construct an estimate of the distance matrix with random effects, followed by an estimate of the curvature. For each of these, we use a triangle filtering constant  $C_{\Delta} = 1.4$  and a minimum clique size seen in Table 2. We lastly apply our test

Physics Sub-field	Number of Nodes (n)	Number of Edges ( $ E $ )
Astrophysics	18771	396160
Condensed Matter Physics	23133	186936
General Relativity	5241	28980
High Energy Particle Physics	12006	237010
High Energy Particle Physics (Theory)	9875	51971

Table 1: Physics Co-authorship network sizes.

to see if the difference in curvature is present across the networks.

Physics Sub-field	Min Clique Size ( $\ell$ )	Number of Cliques of Size $\geq \ell$ (K)	Largest Clique Size
Astrophysics	19	57	57
Condensed Matter Physics	12	52	26
General Relativity	7	44	44
High Energy Particle Physics	14	42	239
High Energy Particle Physics (Theory)	7	42	32

Table 2: Clique size and number of cliques used to estimate distance matrix.

We estimate the following curvatures for each of the networks, along with the following p-values for tests of whether a network has constant curvature. We can plot the structure of the networks in Figure 10.

Physics Sub-field	Curvature Estimate	Constant Curve Test p-value
Astrophysics	-Inf	$1.1 \times 10^{-8}$
Condensed Matter Physics	0.162	0.099
General Relativity	-13.669	0.301
High Energy Particle Physics	-0.758	0.756
High Energy Particle Physics (Theory)	0.142	0.063

Table 3: Curvature estimates from best midpoints and p-values for constant curvature test  $J = 3$

We can additionally plot the smooth truncated ( $c \tanh(\cdot/c)$ ) and filtered estimates of curvature for each region in Figure 11.

We see that Astrophysics and General Relativity are estimated to have a large negative curvature, which however, may not be constant in the case of the Astrophysics citation

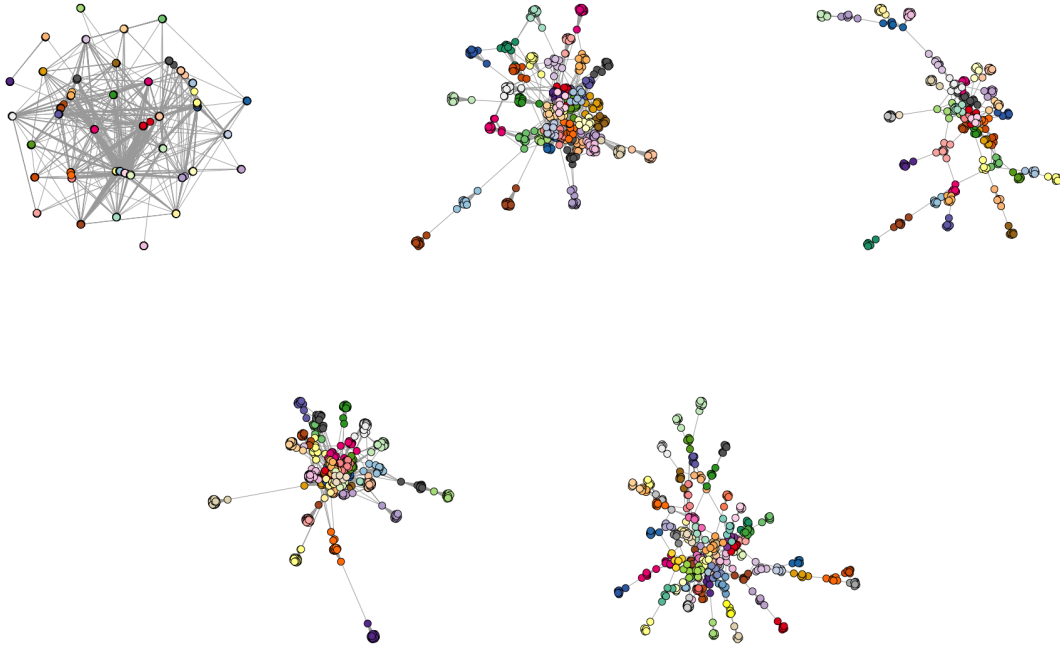


Figure 10: Clique subgraphs of physics co-authorship networks. Ordered from left to right, top to bottom: Astrophysics, Condensed Matter, General Relativity, HEP and HEP (Theory)

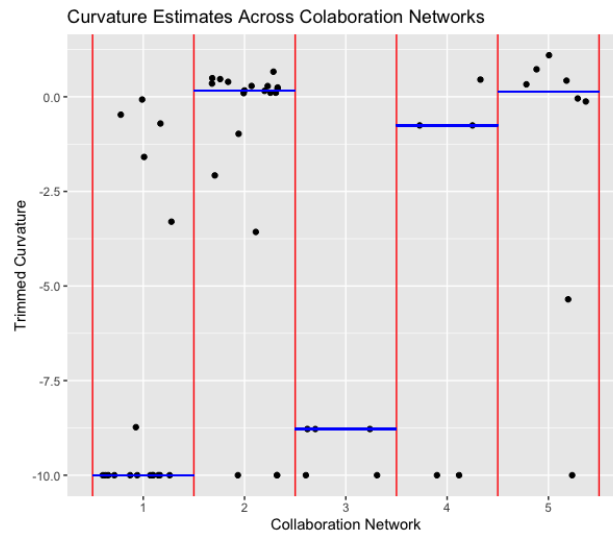
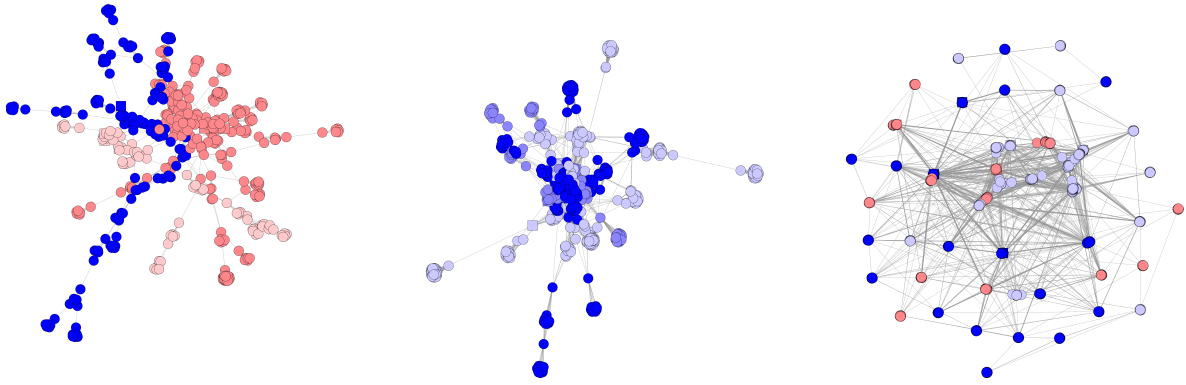


Figure 11: Curvature Estimates of Physics Co-authorship Networks. Networks in order: Astrophysics (1), Condensed Matter Physics (2), General Relativity (3), High Energy Particle Physics (4), High Energy Particle Physics (Theory) (5)



(a) High Energy Particle Physics (Theory) clique curvature labels

(b) High Energy Particle Physics clique curvature labels

(c) Astrophysics clique curvature labels

Figure 12: Cliques Colored to nearest labeled curvature value. Blue, negative and red positive, with  $p$  values of constant curvature decreasing from left to right.

network. In the Astrophysics network, at the best 3 midpoint sets, we estimate curvature to be  $(-\infty, 0.0188, 0.306)$ . The estimate of  $-\infty$  comes from the fact there is a minimum distance of  $d_{xm}$  given the other 3,  $d_{xy}, d_{yz}, d_{xz}$ . If the estimated distance is below this value we call the estimate  $-\infty$ , and similarly  $\infty$  if it is too large. respectively. This highlights the fact that this network appears to have negatively curved, positively curved and flat regions, and therefore models which reflect only a single curvature, may not capture the individual level behaviour of the network very well. In contrast condensed matter physics and HEP physics seem to have a slight curvature, though both are nearly flat networks.

After ruling out the fact that Astrophysics does not have constant curvature, we can apply our KW based test for whether the remaining networks have constant curvature and obtain a  $p$ -value of 0.0011. We see that general relativity has a negative curvature, while the remaining networks tend to have a flatter curvature. We further test whether the curvature is constant amongst either HEP network or condensed matter physics. We find that these curvatures are not significantly different ( $p$ -value 0.1125).

This result suggests that the nature of collaboration tends to be different in these fields. Co-authorship seems to happen between those who have a mutual collaboration in the CMP and HEP while in GR there tends to be more concentrated centre and less influential periphery.

## 6 Application: Multiple change point detection

Another natural question one may seek to answer is whether a change in latent curvature has occurred, and being able to distinguish this from changes in latent positions. Standard Gaussian multiple change point algorithms (for example that of Harchaoui and Lévy-Leduc (2010)) are not suited well to this problem due to the possibility of large outliers.

We apply the method of Fearnhead and Rigaiil (2016) which proposes a multiple change-point detection algorithm under the presence of outliers. For a particular network, we may measure a collection of estimates of the curvature  $\{\widehat{\kappa}_{j,t}\}_{j=1}^{r_t}$ . Under this model, we assume that a network has a constant curvature within a single time point  $t$ . Using the quantile loss function from Fearnhead and Rigaiil (2016) we construct an objective function for the changepoint problem

$$L(\theta) = \sum_{t=1}^T \sum_{j=1}^{r_t} \widetilde{\ell}(\widehat{\kappa}_{j,n_t}, \theta_t)$$

$$\text{Where } \ell(x, y) = \frac{1}{2}|x - y|.$$

In this setting  $\widetilde{\ell}$  is the absolute value difference, however, more general loss functions for quantile regression Koenker and Hallock (2001); Belloni et al. (2011) are also available as options. In multiple change point detection algorithms a penalty of  $\beta$  for the number of segments included is also applied. Let  $J(\theta)$  denote a function of the number of breaks in

the sequence  $\theta$ . Then the full loss function is

$$L(\theta; \beta) = L(\theta) + \beta J(\theta). \quad (15)$$

We then apply this to a simulation setting where we construct a sequence of networks with latent positions.

$$Z_i^{(t)} = \mathcal{F}(Z_i^{(t-1)}, \epsilon_i^{(t)})$$

where  $Z_{(t-1)i}$  is the locations previous position,  $\epsilon_i^{(t)}$  is a noise random variable sampled from the true cluster's density, and  $\mathcal{F}$  stands for the mean on the sphere (the Fréchet mean).

We set three different curvatures

$$\kappa_1 = 1.0 \quad \kappa_2 = 0.15 \quad \kappa_3 = 1.3$$

with time changes at  $t_1 = 18, t_2 = 35$  and total time  $T = 50$ .

As illustrated before, we use the `robseg` package introduced in Fearnhead and Rigaiil (2016) and use the absolute value loss. We see that as  $\ell$  increases, we are able to consistently estimate the true curvature function. We set  $\beta = \log(\text{length}(\boldsymbol{\kappa}))$  where  $\text{length}(\boldsymbol{\kappa})$  is the number of observations, the default recommended by Fearnhead and Rigaiil (2016). We plot the median of the RMSE of the curvature estimate over 200 simulations as a function of the scale using the default tuning parameter from the `Robseg` R package. We plot the results in Figure 13.

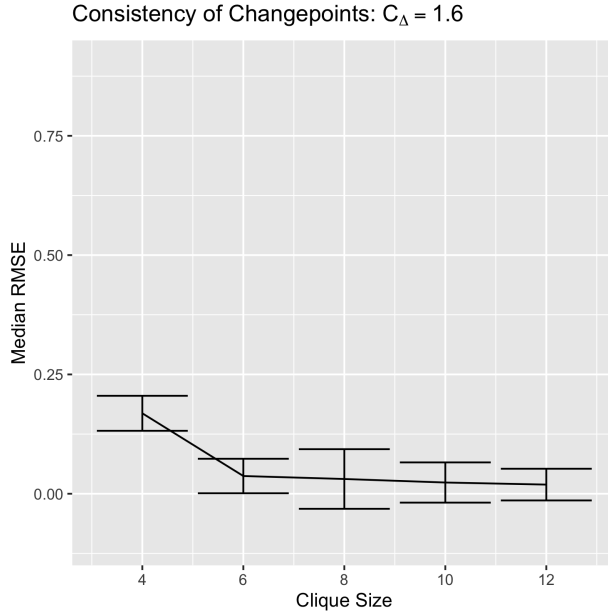


Figure 13: Median RMSE of changepoint curvature estimates.

## 6.1 LANL Netflow and Changepoint detection

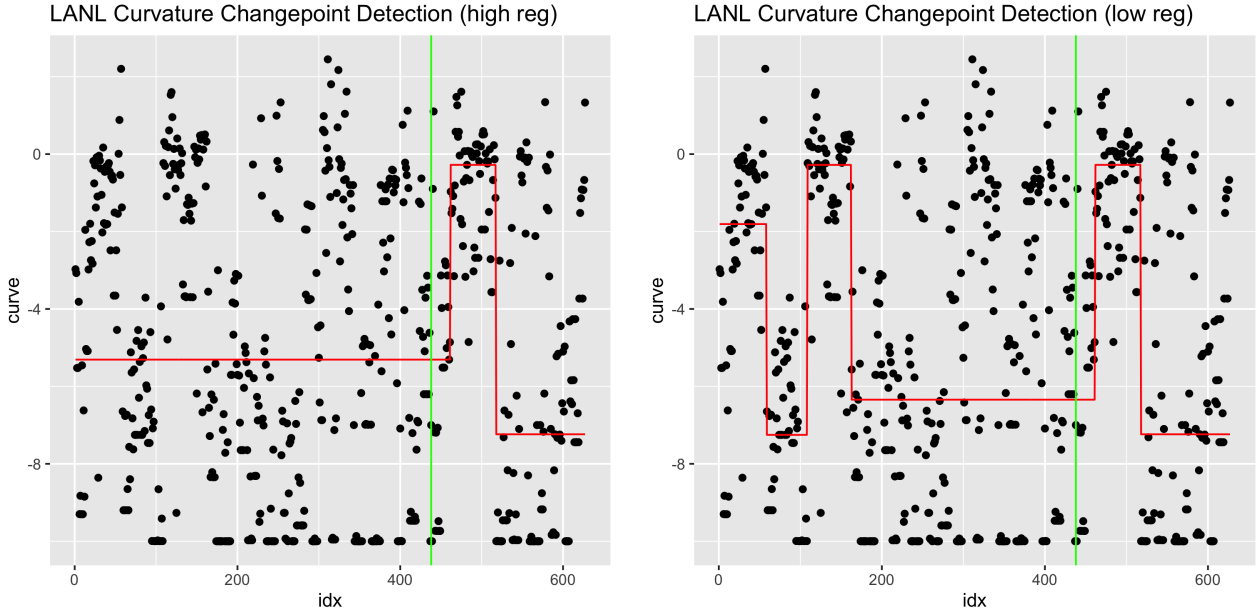
For our second application we apply our estimates of network curvature to Los Alamos Unified Network and Host Dataset, and illustrate that changes in curvature can be used to identify a red team attack. A red team attack is a planned exercise by cybersecurity professionals who hack into a network in order to better detect or prevent breaches of security in the future.

This dataset consists of 89 days of directed communication events between  $n = 27436$  devices in the Los Alamos National Laboratory. The dataset consist of 56 normal days followed by a red team attack beginning on day 57 and continuing to day 89.

Anomaly detection is of great interest for many cybersecurity applications and recently latent space models have been shown to be a promising avenue of detecting changes in node properties (Lee et al., 2019). We take a different approach and illustrate how change point methods can be applied sequential estimates of curvature of this dataset, highlighting the role of global changes of network properties which can be used to detect changes in net-

work behaviour. We illustrate a proof of concept that the changes in network curvature are associated with changes in behaviour.

Edges can be defined in this dataset as messages passed between nodes during a particular time period. In order to maintain enough connections to find cliques, we consider a connection to be formed if any message was passed in the previous 4 days. We then compute the curvature values at each time point and re-scale at each time-point by the median absolute deviation. We scale each estimated value by  $c \tanh(\cdot/c)$  for  $c = 10$  in order to curb strong outliers. We then apply the off the shelf change point algorithm of Fearnhead and Rigaiill (2016). Using a  $C_\Delta = 1.4$  we estimate the curvature at each time frame. We consider a minimum clique size of  $\ell = 5$ . Due to the small number of available cliques, we restrict the random effects to be 0 and compute the corresponding distance matrix.

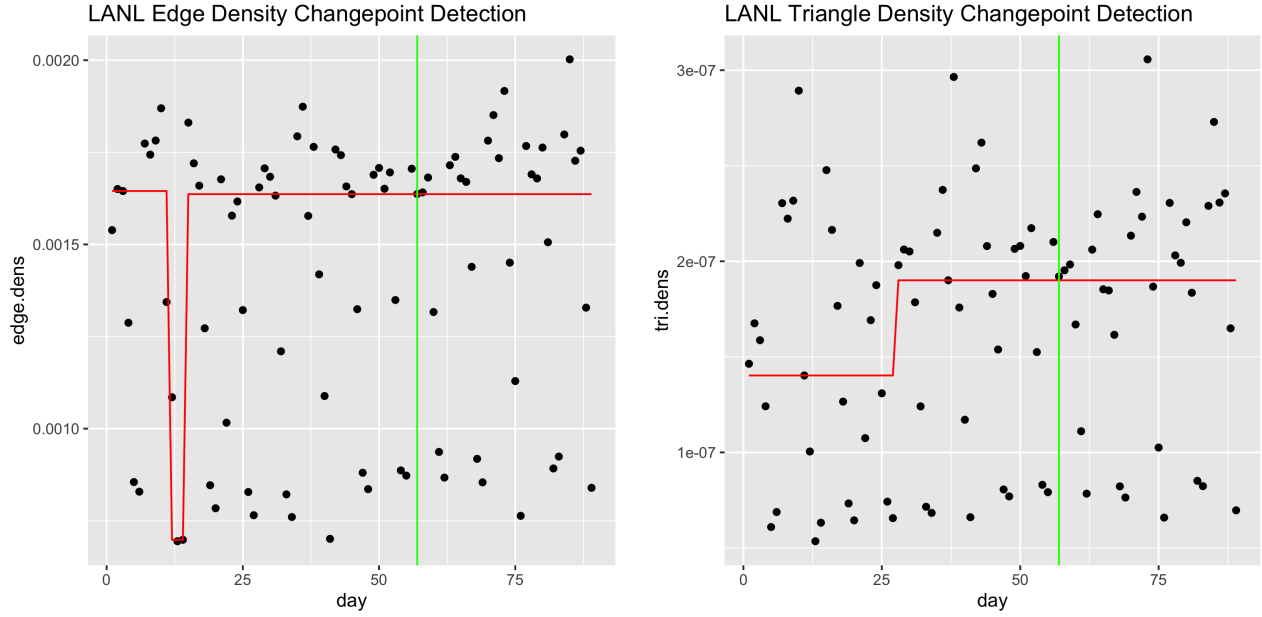


(a) High regularization LANL changes in curvature estimates.

(b) Low regularization LANL changes in curvature estimates.

Figure 14: Two regularization values for LANL Netflow changepoint

In Figure 14 we show that the most substantial changepoint in curvature occurs immediately after the red team attack. In contrast, these changes are much less substantial in Figure 15 when using simple graph motifs from the daily averages.



(a) Edge density change points.

(b) Triangle density change points.

Figure 15: Change points of daily LANL measurements using simple graph motifs

Since the time of detection after the event is most important, we wish to investigate the time after detection as a function of the number of events involved (alarm rate). We show that in Figure 16 that our method achieves a much smaller detection delay given any alarm rate.

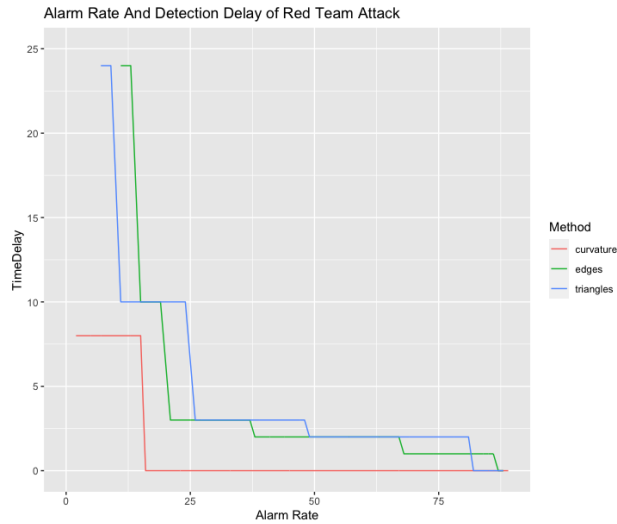


Figure 16: Edge density change points.

Overall, this suggests that models accounting for changes in network curvature may be a

promising avenue for the development of specialised models to detect anomalous events in the online setting.

## 7 Discussion

We presented a method for estimating curvature which is local and asymptotically normal. One concern a reader may have is the fact that we must select what is the best midpoint, given a set of noisy distances. One may naturally worry about selection effects in this case. Since we are selecting the point  $m$  based on its quality of being a good midpoint, rather than selecting for large or small curvature, any selection effects are of minor concern. In practice, we find that when approximately 40 cliques are used then the midpoint bias tends to be rather negligible and we have good midpoint estimates. For example, the midpoint minimization equation (12) which has a value at the true midpoint of 0.5 were found to be 0.5000003, 0.5039226, 0.5004899, 0.5001235, 0.5004292 in the best midpoints of the 5 physics co-authorship networks respectively, suggesting we have near midpoints occurring in real data.

Though we develop a test for detecting whether the curvature is constant on the latent manifold, a natural open question is what should a practitioner do if they find that their data are not represented well by this model. Of course one might instead use non-geometric models such as stochastic block models and their variants. However, this also suggests the development of latent distance models which are not restricted to constant curvature.

Development of such a model class as something which will scale naturally to large networks is of further interest. Computing gradients on arbitrary Riemannian manifolds may prove to be challenging when the positions are in fact latent. One promising approach we plan to investigate in future work is that of product spaces for latent space models. This

geometry has seen considerable success in representation learning tasks Gu et al. (2018); Zhang et al. (2021).

A natural limitation of our method is the interpretation of the curvature parameter  $\kappa$  when a set of points does not lie within a canonical manifold. Our method merely fits for each  $(x, y, z, m)$  the particular constant curvature manifold which will embed these 4 points, and taking the median, will estimate the median of the curvatures of these interpolating spaces. This idea is reminiscent of the manifold learning methods of Li et al. (2017); Li and Dunson (2019) which use spherelets to approximate manifolds rather locally linear approximations of tangent spaces.

When considering the unified network and flow dataset from LANL, we must transform the original dataset of pairs of individuals and times, to one which considers a set of graphs over time. A more realistic model for the data generating mechanism may be one related to a Poisson process (or other point process) with intensity parameters  $\mu_{ij,t} \propto -d_{ij,t}$ .

Future extensions may include methods for fitting models in the product space geometry as well as movement towards statistically consistent node-level definitions of network curvature and a more application focused development of anomaly detection using latent curvature.

## References

- Aliverti, E. and Durante, D. (2019). Spatial modeling of brain connectivity data via latent distance models with nodes clustering. *Statistical Analysis and Data Mining: The ASA Data Science Journal*, 12(3):185–196.
- Andersen, E. D. and Andersen, K. D. (2000). The mosek interior point optimizer for linear

- programming: an implementation of the homogeneous algorithm. In *High performance optimization*, pages 197–232. Springer.
- Banerjee, A., Chandrasekhar, A. G., Duflo, E., and Jackson, M. O. (2013). The Diffusion of Microfinance. *Science*, 341(6144).
- Barkanass, V., Jost, U., and Hancock, E. (2022). Geometric sampling of networks. *Journal of Complex Networks*, 10(4).
- Bassett, D. S., Zurn, P., and Gold, J. I. (2018). On the nature and use of models in network neuroscience. *Nature Reviews Neuroscience 2018 19:9*, 19(9):566–578.
- Begelfor, E. and Werman, M. (2005). The World is not always Flat or Learning Curved Manifolds. *School of Engineering and Computer Science, Hebrew University of Jerusalem., Tech. Rep*, 3(8).
- Belloni, A., Chernozhukov, V., Chetverikov, D., and Fernández-Val, I. (2011). Conditional Quantile Processes based on Series or Many Regressors. *Journal of Econometrics*, 213(1):4–29.
- Blumenthal, L. M. and Gillam, B. E. (1943). Distribution of Points in n-Space. *The American Mathematical Monthly*, 50(3):181.
- Borgatti, S. P., Mehra, A., Brass, D. J., and Labianca, G. (2009). Network analysis in the social sciences. *Science*, 323(5916):892–895.
- Brauchart, J. S., Reznikov, A. B., Saff, E. B., Sloan, I. H., Wang, Y. G., and Womersley, R. S. (2015). Random Point Sets on the Sphere — Hole Radii, Covering, and Separation. *Experimental Mathematics*, 27(1):62–81.
- Burt, R. S. (1992). *Structural holes: The social structure of competition*. Harvard University Press, Cambridge, MA.

- Buskens, V. and Van de Rijt, A. (2008). Dynamics of networks if everyone strives for structural holes. *American Journal of Sociology*, 114(2):371–407.
- Cai, T., Fan, J., and Jiang, T. (2013). Distributions of Angles in Random Packing on Spheres. *Journal of Machine Learning Research*, 14:1837–1864.
- Chamberlain, B. P., Clough, J. R., and Deisenroth, M. P. (2017). Neural Embeddings of Graphs in Hyperbolic Space. In *13th international workshop on mining and learning from graphs held in conjunction with KDD*.
- Chami, I., Ying, R., Ré, C., and Leskovec, J. (2019). Hyperbolic Graph Convolutional Neural Networks. *Advances in Neural Information Processing Systems*, 32.
- Csardi, G., Nepusz, T., et al. (2006). The igraph software package for complex network research. *InterJournal, complex systems*, 1695(5):1–9.
- Durante, F., Fernández-Sánchez, J., and Sempì, C. (2013). A topological proof of Sklar’s theorem. *Applied Mathematics Letters*, 26(9):945–948.
- Farooq, H., Chen, Y., Georgiou, T. T., Tannenbaum, A., and Lenglet, C. (2019). Network curvature as a hallmark of brain structural connectivity. *Nature Communications 2019 10:1*, 10(1):1–11.
- Fearnhead, P. and Rigaiil, G. (2016). Changepoint Detection in the Presence of Outliers. *Journal of the American Statistical Association*, 114(525):169–183.
- Fosdick, B. K., McCormick, T. H., Murphy, T. B., Ng, T. L. J., and Westling, T. (2016). Multiresolution network models. *Journal of Computational and Graphical Statistics*, 28(1):185–196.
- Frechet, M. (1957). Sur la distance de deux lois de probabilité. *CR. Acad Sci. Paris*, 244.
- Fu, A., Narasimhan, B., and Boyd, S. (2020). CVXR: An R package for disciplined convex optimization. *Journal of Statistical Software*, 94(14):1–34.

- Gallot, S., Hulin, D., and Lafontaine, J. (2004). *Riemannian Geometry*. Universitext. Springer Berlin Heidelberg, Berlin, Heidelberg.
- Gilbert, A. C. and Jain, L. (2017). If it ain't broke, don't fix it: Sparse metric repair. In *2017 55th Annual Allerton Conference on Communication, Control, and Computing (Allerton)*, pages 612–619. IEEE.
- Gromov, M., editor (2007). *Metric Structures for Riemannian and Non-Riemannian Spaces*. Birkhäuser Boston.
- Gu, A., Sala, F., Gunel, B., and Ré, C. (2018). Learning mixed-curvature representations in product spaces. In *International Conference on Learning Representations*.
- Harchaoui, Z. and Lévy-Leduc, C. (2010). Multiple change-point estimation with a total variation penalty. *Journal of the American Statistical Association*, 105(492):1480–1493.
- Hoeffding, W. (1940). Masstabvariante Korrelationstheorie. *Schrijl Math. Inst. Univ. Berlin*, 5(6).
- Hoff, P. D., Raftery, A. E., and Handcock, M. S. (2002). Latent space approaches to social network analysis. *Journal of the american Statistical association*, 97(460):1090–1098.
- Killing, W. (1891). Ueber die Clifford-Klein'schen Raumformen. *Mathematische Annalen* 1891 39:2, 39(2):257–278.
- Klingenberg, W. (1995). *Riemannian Geometry*. Walter de Gruyter, 1 edition.
- Koenker, R. and Hallock, K. F. (2001). Quantile Regression. *Journal of Economic Perspectives*, 15(4):143–156.
- Kruskal, W. H. and Wallis, W. A. (1952). Use of Ranks in One-Criterion Variance Analysis. *Journal of the American Statistical Association*, 47(260):583–621.

- Leal, W., Restrepo, G., Stadler, P. F., and Jost, J. (2018). Forman-Ricci Curvature for Hypergraphs. *Advances in Complex Systems*, 24(1).
- Lee, W., McCormick, T. H., Neil, J., Cole, M., Microsoft, S., and Cui, Y. (2019). Anomaly Detection in Large Scale Networks with Latent Space Models. *Technometrics*, pages 1–23.
- Leskovec, J., Kleinberg, J., and Faloutsos, C. (2007). Graph evolution. *ACM Transactions on Knowledge Discovery from Data (TKDD)*, 1(1).
- Li, D. and Dunson, D. B. (2019). Geodesic distance estimation with spherelets. *arXiv preprint arXiv:1907.00296*.
- Li, D., Mukhopadhyay, M., and Dunson, D. B. (2017). Efficient manifold and subspace approximations with spherelets. *arXiv preprint arXiv:1706.08263*.
- Lok, T., Ng, J., Murphy, T. B., Westling, T., McCormick, T. H., and Fosdick, B. (2021). Modeling the social media relationships of Irish politicians using a generalized latent space stochastic blockmodel. *Annals of Applied Statistics*, 15(4):1923–1944.
- Lubold, S., Chandrasekhar, A. G., and McCormick, T. H. (2020). Identifying the latent space geometry of network models through analysis of curvature. Technical report, National Bureau of Economic Research.
- MacDonald, P. W., Levina, E., and Zhu, J. (2022). Latent space models for multiplex networks with shared structure. *Biometrika*, 109(3):683–706.
- Ni, C. C., Lin, Y. Y., Luo, F., and Gao, J. (2019). Community Detection on Networks with Ricci Flow. *Scientific Reports 2019 9:1*, 9(1):1–12.
- Nickel, M. and Kiela, D. (2017). Poincaré Embeddings for Learning Hierarchical Representations. *Advances in Neural Information Processing Systems*, 30.

- Ollivier, Y. (2007). Ricci curvature of Markov chains on metric spaces. *Journal of Functional Analysis*, 256(3):810–864.
- Papadopoulos, L., Porter, M. A., Daniels, K. E., and Bassett, D. S. (2018). Network analysis of particles and grains. *Journal of Complex Networks*, 6(4):485–565.
- Penneec, X. (1999). Probabilities and statistics on Riemannian manifolds: Basic tools for geometric measurements. In *International Workshop on Nonlinear Signal and Image Processing*, pages 194–198, Antalya, Turkey.
- Salter-Townshend, M. and McCormick, T. H. (2017). Latent space models for multiview network data. *Annals of Applied Statistics*, 11(3):1217–1244.
- Samal, A., Pharasi, H. K., Ramaia, S. J., Kannan, H., Saucan, E., Jost, J., and Chakraborti, A. (2021). Network geometry and market instability. *Royal Society Open Science*, 8(2).
- Sandhu, R., Georgiou, T., Reznik, E., Zhu, L., Kolesov, I., Senbabaoglu, Y., and Tannenbaum, A. (2015). Graph Curvature for Differentiating Cancer Networks. *Nature Scientific Reports*, 5(1):1–13.
- Sandhu, R. S., Georgiou, T. T., and Tannenbaum, A. R. (2016). Ricci curvature: An economic indicator for market fragility and systemic risk. *Science Advances*, 2(5).
- Saucan, E., Samal, A., and Jost, J. (2020). A Simple Differential Geometry for Complex Networks. *Network Science*, 9(S1):S106–S133.
- Schoenberg, I. J. (1935). Remarks to Maurice Frechet’s Article “Sur La Definition Axiomatique D’Une Classe D’Espace Distances Vectoriellement Applicable Sur L’Espace De Hilbert. *The Annals of Mathematics*, 36(3):724.
- Sia, J., Jonckheere, E., and Bogdan, P. (2019). Ollivier-Ricci Curvature-Based Method

- to Community Detection in Complex Networks. *Nature, Scientific Reports 2019 9:1*, 9(1):1–12.
- Sklar, A. (1959). Fonctions de repartition a n dimensions et leurs marges. *Publications de l'Institut de statistique de l'Université de Paris*, 8:229–231.
- Smith, A. L., Asta, D. M., and Calder, C. A. (2017). The Geometry of Continuous Latent Space Models for Network Data. *Statistical Science*, 34(3):428–453.
- Sweet, T. and Adhikari, S. (2020). A Latent Space Network Model for Social Influence. *Psychometrika*, 85(2):251–274.
- van der Hoorn, P., Cunningham, W. J., Lippner, G., Trugenberg, C., and Krioukov, D. (2020). Ollivier-Ricci curvature convergence in random geometric graphs. *Physical Review Research*, 3(1).
- van der Vaart, A. (1998). *Asymptotic Statistics*. Cambridge University Press.
- Volz, E. M., Miller, J. C., Galvani, A., and Meyers, L. (2011). Effects of Heterogeneous and Clustered Contact Patterns on Infectious Disease Dynamics. *PLOS Computational Biology*, 7(6):e1002042.
- Zhang, S., Tay, Y., Jiang, W., Juan, D.-c., and Zhang, C. (2021). Switch spaces: learning product spaces with sparse gating. *arXiv preprint arXiv:2102.08688*.

# A Proofs of Theorems

## A.1 Proof of Lemma 2.2

*Proof.* Consider first a set of 3 points on  $(x, y, z) \in \mathbb{S}^p$  which are not co-linear. We can define an orthogonal matrix (rotation matrix)  $Q \in \mathbb{R}^{p+1 \times p+1}$  which we will first construct a rotational isometry, then use a result consisting of fixed point isometries .

**Theorem A.1** (Theorem 1.10.15 in Klingenberg (1995)). *If  $f : (\overline{M}, \overline{g}) \rightarrow (\overline{M}, \overline{g})$  is an isometry on a Riemannian manifold, then the fixed point set of  $f$  forms a totally geodesic submanifold.*

WLOG let  $x = (1, 0, \dots, 0)$ . We define the orthogonal rotation matrix  $Q$  via the following. Let  $q_i$  denote the  $i^{th}$  un-normalized column vector of  $Q$ . We the define the following first 3 basis functions

$$\begin{aligned}q_1 &= [1, 0, \dots, 0]^T \\q_2 &= y - (y^T q_1)q_1 \\q_3 &= z - \frac{(z^T q_2)}{\|q_2\|_2}q_2 - (z^T q_1)q_1\end{aligned}$$

Then normalizing each of these vectors to construct the columns of  $Q$  and completing the orthonormal basis with any remaining orthogonal basis vectors of  $\mathbb{R}^p$ , and we have constructed an orthogonal matrix  $Q$  and  $Q^T Q = I = Q Q^T$ /. Thus we have defined an isomor-

phism  $f_1(\cdot) : \mathbb{S}^p \mapsto \mathbb{S}^p$  where

$$\begin{aligned}
 f_1(x) &= Q^T x \\
 d(f_1(x), f_1(y)) &= \frac{1}{\sqrt{\kappa}} \operatorname{acos} (f_1(x)^T f_1(y)) \\
 &= \frac{1}{\sqrt{\kappa}} \operatorname{acos} (x^T Q Q^T y) \\
 &= \frac{1}{\sqrt{\kappa}} \operatorname{acos} (x^T y) \\
 &= d(f_1(x), f_1(y))
 \end{aligned}$$

hence this rotation is an isomorphism. Then let  $f_2(x) = (x_0, x_1, x_2, -x_3, -x_4, \dots, -x_p)$  denote an additional isomorphism. Since the composition of isomorphisms is also an isomorphism, we can define a totally geodesic submanifold of dimension 2 which consists of the solution set to  $Q^T = [c_1, c_2, c_3, 0, 0, \dots, 0]^T$  for some  $c_1, c_2, c_3$  by Theorem A.1. Then clearly,  $x, y, z$  are all fixed points of this isomorphism by construction, and hence any three points can be contained within a totally geodesic submanifold of dimension 2 of the corresponding curvature.

The proofs for  $\mathbb{E}^p$  and  $\mathbb{H}^p$  follows this argument identically and thus the proof is complete. □

## A.2 Proof of Theorem 2.3

*Proof.* Any 3 points  $(x, y, z)$  can be embedded isometrically in a totally geodesic submanifold of dimension 2 when  $\mathcal{M}^p(\kappa)$  is a canonical manifold due to the symmetry of each of the spaces.

**Case 1: Spherical.** Under the spherical model, first place the midpoint at the origin.

Next, given  $d_{yz}$  place point  $y$  at the point  $(y_0, y_1, 0)$  where  $y_1 = \sqrt{1 - y_0^2}$ . Then  $y_0 =$

$\cos(\sqrt{\kappa}\frac{d_{yz}}{2})$ . Next we place point  $z$  at  $z = (z_0, z_1, 0)$  where  $z_0 = y_0$  and  $z_1 = -y_1$ . Third we solve for the locations of  $x$  such that  $d_{xm}, d_{xy}, d_{xz}$  are satisfied.

We continue with  $x = (x_0, x_1, x_2)$ . We can set  $x_0 = \cos(\sqrt{\kappa}\frac{d_{xm}}{2})$ . Next  $x_1$  can be solved by letting

$$\begin{aligned}\cos(\sqrt{\kappa}d_{xy}) &= x_0y_0 + x_1y_1 \\ &= \cos(\sqrt{\kappa}d_{xm}) \cos(\sqrt{\kappa}d_{yz}/2) + x_1 \sin(\sqrt{\kappa}d_{yz}/2)\end{aligned}$$

Similarly

$$\begin{aligned}\cos(\sqrt{\kappa}d_{xz}) &= x_0z_0 + x_1z_1 \\ &= \cos(\sqrt{\kappa}d_{xm}) \cos(\sqrt{\kappa}d_{yz}/2) - x_1 \sin(\sqrt{\kappa}d_{yz}/2)\end{aligned}$$

solving for  $x_1$  results in:

$$\frac{\cos(\sqrt{\kappa}d_{xy}) - \cos(\sqrt{\kappa}d_{xm}) \cos(\sqrt{\kappa}d_{yz}/2)}{\cos(\sqrt{\kappa}d_{xz}) - \cos(\sqrt{\kappa}d_{xm}) \cos(\sqrt{\kappa}d_{yz}/2)} = -1$$

which can be further rearranged to

$$2 \cos(d_{xm}\sqrt{\kappa}) - \text{Sec}(\frac{d_{yz}}{2}\sqrt{\kappa})(\cos(d_{xy}\sqrt{\kappa}) + \cos(d_{xz}\sqrt{\kappa})) = 0$$

We then normalize this by the curvature value  $\frac{1}{\kappa}$  which allows for  $g(\kappa, d)$  to be a continuous function of  $\kappa$  from the hyperbolic  $\kappa < 0$  to spherical space  $\kappa > 0$ .

**Case 2: Hyperbolic.** The proof of the hyperbolic case follows an identical method to the spherical case.

Remark: Under the limit as  $\kappa \rightarrow 0$  we find that  $\lim_{\kappa \rightarrow 0} g(\kappa, d) = \frac{1}{2}d_{xy}^2 + \frac{1}{2}d_{xz}^2 - \frac{1}{4}d_{yz}^2 - d_{xm}^2$  which gives exactly the parallelogram law in Euclidean space. This also highlights the ne-

cessity that the term  $\frac{1}{\kappa}$  plays in maintaining a smooth equation as a function of  $\kappa$  through 0. □

### A.3 Proof of Theorem 2.4

*Proof.* We will use the implicit function theorem to construct an implicit function for which we can later apply a delta method. We first note that  $g(\kappa, d)$  is continuously differentiable when  $\sqrt{\kappa} < \frac{\text{acos}(\pi)}{d_{yz}}$ . This boundary however corresponds to the maximum distance allowed on a sphere, as given by two anti-polar points. Therefore to apply the implicit function theorem, what remains is

$$\frac{\partial}{\partial \kappa} g(\kappa, d) \neq 0.$$

which we assume holds by (B3). By the implicit function theorem there exists an open neighbourhood  $\mathcal{D} \in \mathbb{R}^4$  and a function  $f(d)$  such that  $\kappa = f(d)$  and  $g(f(d), d)$ . Furthermore:

$$\nabla_d f(d) = - \left( \frac{\partial g(\kappa, d)}{\partial \kappa} \right)^{-1} [\nabla_d g(\kappa, d)]$$

Therefore by the delta method:

$$\begin{aligned} \sqrt{r(n)}(\hat{\kappa} - \kappa) &= \sqrt{r(n)}(f(\hat{d}) - f(d)) \\ &\rightarrow_W N(0, \nabla g(d)^T \Sigma \nabla g(d)) \end{aligned}$$

And by the implicit function theorem:

$$\nabla g(d)^T \Sigma \nabla g(d) = \left( \frac{\partial g(\kappa, d)^2}{\partial \kappa} \right)^{-1} [\nabla_d g(\kappa, d)^T \Sigma \nabla_d g(\kappa, d)]$$

**Remark:** This form is very similar to the usual standard asymptotic normality proofs for  $Z$  estimators as in van der Vaart (1998). However, the main difference is in the fact that we are not averaging the estimating function, but rather plugging in a distance estimate which is asymptotically normal.

We find that in practice, condition (B3) holds, however, for some distances that are plugged in, particularly those which may not satisfy a midpoint exactly may result in the root of the estimating function be the root of its partial derivative. In fact, in the Euclidean case, according to the Taylor series expansion at  $\kappa = 0$

$$g(\kappa; d) = \frac{1}{\kappa} \left( \left( \frac{d_{xy}^2}{2} + \frac{d_{xz}^2}{2} - d_{xm}^2 - \frac{d_{yz}^2}{4} \right) \kappa + \left( \frac{d_{xm}^2}{12} - \frac{5d_{yz}^2}{192} + \frac{1}{16} d_{yz}^2 (d_{xy}^2 + d_{xz}^2) - \frac{1}{24} (d_{xy}^2 + d_{xz}^2) \right) \kappa^2 + \mathcal{O}(\kappa^3) \right).$$

Clearly at  $\kappa = 0$  the solution reduces to the parallelogram law ( $\frac{d_{xy}^2}{2} + \frac{d_{xz}^2}{2} - d_{xm}^2 - \frac{d_{yz}^2}{4} = 0$ ).

When we substitute in the corresponding solution at  $\kappa = 0$ .

$$\begin{aligned} \left. \frac{\partial}{\partial \kappa} g(\kappa; d) \right|_{\kappa=0} &= -\frac{1}{48} (d_{yz}^4 - 2d_{yz}^2 (d_{xz}^2 + (d_{xy}^2) + (d_{xz}^2 - d_{xy}^2)^2) \\ &= -\frac{1}{48} ((d_{yz} + d_{xz} + d_{xy})(d_{yz} - d_{xz} - d_{xy})(d_{yz} - d_{xz} + d_{xy})(d_{yz} + d_{xz} - d_{xy})) \end{aligned}$$

Clearly as long as the triangle inequality is satisfied strictly for  $x, y, z$  then  $\left. \frac{\partial}{\partial \kappa} g(\kappa; d) \right|_{\kappa=0} > 0$ . However, if the triangle inequality is not strict, i.e  $x, y, z$  are co-linear, and  $d_{ij} = d_{ik} + d_{kj}$  for  $(i, j, k)$  being some permutation of  $(x, y, z)$ , then  $\left. \frac{\partial}{\partial \kappa} g(\kappa; d) \right|_{\kappa=0} = 0$ . For  $\kappa \neq 0$  we do not have simple closed form expressions for  $\left. \frac{\partial}{\partial \kappa} g(\kappa; d) \right|_{\kappa=0}$  and thus we leave (B3) as an

assumption, however, we believe this trend to hold in the other geometries.

□

## A.4 Proof of Lemma 3.1

The proof draws on a similar structure to that of the consistency result of Lubold et al. (2020).

*Proof.* Let  $\epsilon_\delta := \{\Delta_\ell < \delta\}$ . We wish to show that:

$$\lim_{\ell \rightarrow \infty} \frac{P(\epsilon_{\delta_\ell} | C_\ell)}{P(\epsilon_{\delta_\ell}^c | C_\ell)} \rightarrow \infty$$

for  $\delta = O(\exp(-\ell))$ .

This is so we can integrate out  $\nu$ , then taking the ratio, allows us to ignore  $\nu$ .

$$\begin{aligned} P(C_\ell | \epsilon_{\delta_\ell}) &= \int \int_{\epsilon_\delta} \exp\left(-\binom{\ell}{2} \bar{d}(z)\right) \exp\left(-\binom{\ell}{2} \bar{\nu}\right) dP(Z) dP_\nu(\nu) \\ &= \Psi(P_\nu) \int_{\epsilon_\delta} \exp\left(-\binom{\ell}{2} \bar{d}(z)\right) dP(Z) \\ \text{where } \Psi(P_\nu) &= \int \exp\left(-\binom{\ell}{2} \bar{\nu}\right) dP_\nu(\nu). \end{aligned}$$

This can be developed analogously for  $P(C_\ell | \epsilon_{\delta_\ell}^c)$  allowing us to ignore the random effects in this analysis. Next, since

$$\frac{P(\epsilon_{\delta_\ell} | C_\ell)}{P(\epsilon_{\delta_\ell}^c | C_\ell)} = \frac{1}{P(\epsilon_{\delta_\ell}^c | C_\ell)}$$

This would imply  $P(\epsilon_{\delta_\ell}^c | C_\ell) \rightarrow 0$  and hence

$$\Delta_\ell | C_\ell = o_P(\exp(-\tilde{\mu}_d \ell))$$

Then consider the ball of radius  $\frac{\delta}{2}$  at a point  $q \in B(\delta, q)$ . This describes one set of points for which all points have a maximal distance of  $\delta$ . Then the event  $\mathbb{B}(\delta, q)$ , the event that  $\ell$  independent points all lie in this ball. Hence  $P(C_\ell | \epsilon_{\delta_\ell}^c) \geq (c_2 (\frac{\delta_\ell}{2})^p)^\ell$ .

Furthermore

$$P(C_\ell | \epsilon_{\delta_\ell}^c) \leq \int \exp\left(-\binom{\ell}{2} \bar{d}\right) dP_{\bar{d}}(\bar{d})$$

where  $\bar{d} = \frac{1}{\binom{\ell}{2}} \sum_{i < j} d(Z_i, Z_j)$ . Let  $\mu_d = \mathbb{E}[d(Z_i, Z_j)]$ . This is due to the fact  $\epsilon_\delta$  denotes the event that  $\Delta > d$  it is reasonable that  $P(C_\ell | \epsilon_\delta^c) \geq P(C_\ell)$  since we are excluding the most likely events

Then since  $\bar{d} \rightarrow_P \mathbb{E}[d(Z_i, Z_j)] = \mu_d$ , for any  $\tilde{\mu}_d < \mu_d$

$$\lim_{\ell \rightarrow \infty} \frac{\exp\left(-\binom{\ell}{2} \tilde{\mu}_d\right)}{\int \exp\left(-\binom{\ell}{2} \bar{d}\right) dP(\bar{d})} \geq 1$$

Returning to the computation of the ratio of probabilities,

$$\begin{aligned}
\frac{P(\epsilon_{\delta_\ell}|C_\ell)}{P(\epsilon_{\delta_\ell}^c|C_\ell)} &= \frac{P(C_\ell|\epsilon_{\delta_\ell})}{P(C_\ell|\epsilon_{\delta_\ell}^c)} \frac{P(\epsilon_{\delta_\ell})}{1 - P(\epsilon_{\delta_\ell})} \\
&\geq \frac{P(C_\ell|\epsilon_{\delta_\ell})}{P(C_\ell|\epsilon_{\delta_\ell}^c)} \frac{1}{2} P(\epsilon_{\delta_\ell}) \\
&\geq \frac{P(C_\ell|\epsilon_{\delta_\ell})}{P(C_\ell|\epsilon_{\delta_\ell}^c)} c_2^\ell \left(\frac{\delta}{2}\right)^{p\ell} \\
&\geq \frac{\exp(-\binom{\ell}{2}\delta)}{P(C_\ell|\epsilon_{\delta_\ell}^c)} c_2^\ell \left(\frac{\delta}{2}\right)^{p\ell}
\end{aligned}$$

Therefore for large  $\ell$

$$\begin{aligned}
\frac{P(\epsilon_{\delta_\ell}|C_\ell)}{P(\epsilon_{\delta_\ell}^c|C_\ell)} &\geq \frac{\exp(-\binom{\ell}{2}\delta)}{\exp(-\binom{\ell}{2}\tilde{\mu}_d)} \frac{\exp(-\binom{\ell}{2}\tilde{\mu}_d)}{\int \exp(-\binom{\ell}{2}\bar{d}) dP(\bar{d})} c_2^\ell \left(\frac{\delta}{2}\right)^{p\ell} \\
&\geq \frac{\exp(-\binom{\ell}{2}\delta)}{\exp(-\binom{\ell}{2}\tilde{\mu}_d)} c_2^\ell \left(\frac{\delta}{2}\right)^{p\ell} \\
&\quad \exp\left(-\binom{\ell}{2}\delta + \binom{\ell}{2}\tilde{\mu}_d + \ell \log(C) + p\ell \log(\delta) - p\ell \log(2)\right)
\end{aligned}$$

therefore  $\delta \rightarrow 0$  the dominant term is  $\binom{\ell}{2}\tilde{\mu}_d$  and therefore for any  $\delta = o(\exp(-\tilde{\mu}_d))$  then

$$\frac{P(\epsilon_{\delta_\ell}|C_\ell)}{P(\epsilon_{\delta_\ell}^c|C_\ell)} \xrightarrow{\ell \rightarrow \infty} \infty$$

and therefore the proof is complete. □

## A.5 Proof of Lemma 3.2

At a high level, the proof structure is nearly identical to Lemma 3.1, however we swap the roles of  $\nu$  and  $d(Z_i, Z_j)$ .

*Proof.* Let  $\epsilon_\delta = \{\min_{i \in \{1, 2, \dots, \ell\}} \nu_i < -\delta\}$

If  $f_\nu(\nu)$  is smooth and has left side derivative around 0 then for small enough  $\delta$

$F_\nu(\nu > -\delta) \geq c_3\delta$  as in our assumption. As in the previous method we similarly take the ratio and integrate out  $\Psi(P_d)$ .

Then consider the set  $[-\delta_\ell, 0]$ . Then  $P(\varepsilon_{\delta_\ell}^c) \geq (c_3(\delta_\ell))^\ell$ .

Furthermore

$$P(C_\ell|\varepsilon_{\delta_\ell}^c) \leq \int \exp\left(\binom{\ell}{2}\bar{\nu}\right) dP_\nu(\nu)$$

where  $\nu d = \frac{1}{\ell} \sum_{i < j} \nu$  Let  $\mu_\nu = \mathbb{E}[\nu]$ . This is due to the fact  $\varepsilon_\delta$  denotes the event that  $\min_i \nu < -\delta$  it is reasonable that  $P(C_\ell|\varepsilon_\delta^c) \geq P(C_\ell)$  since we are excluding the events most likely to create a clique.

Then since  $\bar{\nu} \rightarrow_P \mu_\nu$ , for any  $0 > \tilde{\mu}_\nu < \mu_\nu$

$$\lim_{\ell \rightarrow \infty} \frac{\exp\left(\binom{\ell}{2}\tilde{\mu}_\nu\right)}{\int \exp\left(\binom{\ell}{2}\bar{\nu}\right) dP_{\bar{\nu}}(\bar{\nu})} \geq 1$$

Returning to the computation of the ratio of probabilities,

$$\begin{aligned} \frac{P(\varepsilon_{\delta_\ell}|C_\ell)}{P(\varepsilon_{\delta_\ell}^c|C_\ell)} &= \frac{P(C_\ell|\varepsilon_{\delta_\ell})}{P(C_\ell|\varepsilon_{\delta_\ell}^c)} \frac{P(\varepsilon_{\delta_\ell})}{1 - P(\varepsilon_{\delta_\ell})} \\ &\geq \frac{P(C_\ell|\varepsilon_{\delta_\ell})}{P(C_\ell|\varepsilon_{\delta_\ell}^c)} \frac{1}{2} P(\varepsilon_{\delta_\ell}) \\ &\geq \frac{P(C_\ell|\varepsilon_{\delta_\ell})}{P(C_\ell|\varepsilon_{\delta_\ell}^c)} c_3^\ell (\delta)^\ell \\ &\geq \frac{\exp\left(-\binom{\ell}{2}\delta\right)}{P(C_\ell|\varepsilon_{\delta_\ell}^c)} c_3^\ell (\delta)^\ell \end{aligned}$$

Therefore for large  $\ell$

$$\begin{aligned} \frac{P(\varepsilon_{\delta_\ell}|C_\ell)}{P(\varepsilon_{\delta_\ell}^c|C_\ell)} &\geq \frac{\exp(-\binom{\ell}{2}\delta)}{\exp(\binom{\ell}{2}\tilde{\mu}_\nu)} \frac{\exp(\binom{\ell}{2}\tilde{\mu}_\nu)}{\int \exp(\binom{\ell}{2}\bar{\nu}) dP(\bar{\nu})} c_3^\ell (\delta)^\ell \\ &\geq \frac{\exp(-\binom{\ell}{2}\delta)}{\exp(\binom{\ell}{2}\tilde{\mu}_\nu)} c_3^\ell (\delta)^\ell \\ &\quad \exp\left(-\binom{\ell}{2}\delta + \binom{\ell}{2}\tilde{\mu}_\nu + \ell \log(c_3) + p\ell \log(\delta) - p\ell \log(2)\right) \end{aligned}$$

therefore  $\delta \rightarrow 0$  the dominant term is  $\binom{\ell}{2}\tilde{\mu}_\nu$  and therefore for any  $\delta = o(\exp(-\tilde{\mu}_\nu))$  then

$$\frac{P(\varepsilon_{\delta_\ell}|C_\ell)}{P(\varepsilon_{\delta_\ell}^c|C_\ell)} \xrightarrow{\ell \rightarrow \infty} \infty$$

and therefore the proof is complete. □

## A.6 Proof of Theorem 3.4

*Proof.* The proof here is a straightforward application of the plug in estimator of  $\hat{p}_{XY}$  and the set of random effects  $\hat{\gamma}_{X/Y}$ . Then by the Lindeberg-Feller CLT:

$$\sqrt{\ell^2 \sigma_\ell} (\hat{p}_{XY} - p_{XY}) \rightarrow_d N(0, 1)$$

Plugging this in to our definition of distance

$$\begin{aligned} \hat{d}_{XY} &= -\log(\hat{p}_{XY}) + \hat{\gamma}_X + \hat{\gamma}_Y \\ \sqrt{\ell^2} \hat{d}_{XY} &= -\sqrt{\ell^2} \log(\hat{p}_{XY}) + \sqrt{\ell^2} \hat{\gamma}_X + \sqrt{\ell^2} \hat{\gamma}_Y \\ &= -\sqrt{\ell^2} \log(\hat{p}_{XY}) + o_P(1) \end{aligned}$$

And by the delta method:

$$\sqrt{\ell^2 \frac{\sigma_\ell}{p_{XY}}} \left( \widehat{d}_{XY} - d_{XY} \right) \rightarrow_d N(0, 1)$$

□

## A.7 Proof of Theorem 2.6

In order to prove Theorem 2.6 we prove a series of lemmas.

Let  $F$  denote a marginal distribution (in our case that of  $\Xi(m)$ ) and let  $X_i$  be a random variable with distribution function  $F$ . By Sklar's Theorem (Sklar, 1959; Durante et al., 2013) we can express the joint distribution ( $H$ ) of a vector of correlated  $X$ ,  $H$  as

$$\begin{aligned} H(\mathbf{x}) &= P(X_1 \leq x_1, X_2 \leq x_2, \dots, X_n \leq x_n) \\ &= \mathbb{C}(F(x_1), F(x_2), \dots, F(x_n)) \end{aligned}$$

where  $\mathbb{C}$  is a copula for the joint distribution. In order to prove this theorem, we prove a series of lemmas.

**Lemma A.2.** *For a set of random variables  $X_i$  with equal marginal distribution, with arbitrary correlation structure denoted via copula  $\mathbb{C}$ , then  $\widehat{\mathbb{M}}(X) = F^{-1}(\widehat{\mathbb{M}}(U))$  where  $U \sim \mathbb{C}$*

*Proof.* We can express  $X = F^{-1}(U)$  where  $U$  is sampled from the copula  $\mathbb{C}$ . Then if  $n$  is odd,  $X_{((n+1)/2)}$  is the median, and clearly  $X_{(i)} = F^{-1}(U_{(i)})$  with the subscript  $(i)$  denoting the  $i^{\text{th}}$  order statistic. Now consider  $n$  which is even. If  $z$  is a median of  $U$  then

$z \in [U_{(n/2)}, U_{(n/2+1)}]$  then

$$\begin{aligned}
z &\in [U_{(n/2)}, U_{(n/2+1)}] \\
\iff F^{-1}(z) &\in [F^{-1}(U_{(n/2)}), F^{-1}(U_{(n/2+1)})] \\
\iff F^{-1}(z) &\in [X_{(n/2)}, X_{(n/2+1)}]
\end{aligned}$$

Hence medians of  $X$ . Hence medians of the underlying uniform distribution are mapped to the median of the observed variables.  $\square$

This lemma suggests that if we take the median of the underlying generative uniforms of the set of correlated random variables. We next investigate an upper bound on the union of events.

**Lemma A.3.** *Consider a set  $A_I = \cap_{i \in I} \{U_i \leq z\}$  where  $I$  is a subset of  $\{1, 2, \dots, n\}$ . Consider a sequence of sets  $A_j$  such that any pair of  $j, j'$  contain at least 1 overlapping index. Then*

$$\mathbb{C}(\cup A_j) \leq \mathbb{W}(\cup A_j) \tag{16}$$

where  $\mathbb{W}$  is the perfectly collinear measure corresponding to the upper Fréchet Hoeffding Bound (Frechet, 1957; Hoeffding, 1940).

*Proof.* We prove this by induction. Consider the base case  $A_1, A_2$ . Suppose there exists some copula  $\mathbb{Q}$  such that  $\mathbb{Q}(A_1 \cup A_2) > \mathbb{W}(A_1 \cup A_2)$ . Firstly under  $\mathbb{W}$

$$\begin{aligned}
\mathbb{W}(A_1 \cup A_2) &= \mathbb{W}(A_1) + \mathbb{W}(A_2) - \mathbb{W}(A_1 \cap A_2) \\
&= \min\{1, z\} + \min\{1, z\} - \min\{1, z\} \\
&= z + z - z \\
&= z
\end{aligned}$$

Then since  $\{A_j, \cup A_{j'}\} \subset \{U_k \leq z\}$  for some index  $k$ . Then

$$\mathbb{Q}(A_1 \cup A_2) \leq \mathbb{Q}(U_k \leq z)$$

However, then  $\mathbb{Q}(U_k \leq z) > z$  and thus  $\mathbb{Q}$  is not a copula, so the base case must be true.

Now suppose the following holds for any  $\mathbb{Q}$ .

$$\mathbb{Q}(\cup_{j=1}^n A_j) \leq \mathbb{W}(\cup_{j=1}^n A_j)$$

for some  $n$ . Denote  $B = \cup_{j=1}^n A_j$  then we show:

$$\mathbb{Q}(B \cup A_{n+1}) \leq \mathbb{W}(B \cup A_{n+1})$$

Suppose that there exists  $\mathbb{Q}$  such that  $\mathbb{Q}(B \cup A_{n+1}) > \mathbb{W}(B \cup A_{n+1})$

$$\mathbb{W}(B \cup A_{n+1}) = \mathbb{W}(B) + \mathbb{W}(A_{n+1}) - \mathbb{W}(B \cap A_{n+1})$$

Clearly,  $\mathbb{W}(B) = z$ ,  $\mathbb{W}(A_{n+1}) = z$  and  $\mathbb{W}(B \cap A_{n+1}) = z$ . Then  $\mathbb{Q}(B \cup A_{n+1}) = \mathbb{Q}(B) + \mathbb{Q}(A_{n+1}) - \mathbb{Q}(B \cap A_{n+1})$ . Therefore

$$\mathbb{Q}(B \cup A_{n+1}) \leq z + \underbrace{\mathbb{Q}(A_{n+1}) - \mathbb{Q}(B \cap A_{n+1})}_{\geq 0}$$

which generates a contradiction hence

$$\mathbb{Q}(B \cup A_{n+1}) \leq \mathbb{W}(B \cup A_{n+1})$$

□

**Lemma A.4.** *For any copula measure,  $\mathbb{C}$*

$$\mathbb{C}(\widehat{\mathbb{M}}(U) \leq z) \leq 2z \tag{17}$$

*Proof.* Define the events  $A_j$  as in Lemma A.3 of size  $\lceil n/2 \rceil$ . Then the event  $\{\widehat{\mathbb{M}}(U) \leq z\}$  is equal to the union of all such  $A_j$  as the median will be equivalent to the case when at least half of all uniforms are below  $z$ . We can partition  $A_j$  into two sets  $S_1, S_2$  for which any two pairs of  $A_j$  in a set have at least one overlapping index. This can be done by taking all the sets  $A_j$  containing  $\{U_1 \leq z\}$  in their index and placing them into set  $S_1$ . Then all other sets must be placed in set  $S_2$ . Since there are  $(n - 1)$  possible remaining indices  $\{2, 3, \dots, n\}$  available for  $S_2$  then any two events must have an overlapping index by the pigeonhole principle. Therefore

$$\begin{aligned} \mathbb{C}(\widehat{\mathbb{M}}(U) \leq z) &= \mathbb{C}(\cup A_i) \\ &= \mathbb{C}(S_1 \cup S_2) \\ &\leq \mathbb{C}(S_1) + \mathbb{C}(S_2) \text{ Union Bound} \\ &\leq \mathbb{W}(S_1) + \mathbb{W}(S_2) \text{ Lemma A.3} \\ &= 2z \end{aligned}$$

□

For our theorem, this is all we need, but a corollary immediately follows. This relates the concentration of any set of arbitrarily correlated uniforms to the concentration of a singular component element.

**Corollary A.5.** *For any copula  $\mathbb{C}$ .*

$$\mathbb{C}(|\widehat{\mathbb{M}}(U) - 1/2| > \epsilon) \leq 2P(|U - 1/2| > \epsilon) \tag{18}$$

*Proof.*  $P(|U - 1/2| > \epsilon)$  is simply the marginal distribution of a uniform distribution.

$$P(|U - 1/2| > \epsilon) = \max\{1 - 2\epsilon, 0\}$$

Next we note that

$$\{|\widehat{\mathbb{M}}(U) - 1/2| > \epsilon\} = \{\widehat{\mathbb{M}}(U) < 1/2 - \epsilon\} \cap \{\widehat{\mathbb{M}}(U) > 1/2 + \epsilon\}$$

Note that we can define  $1 - V = U$  where the measure of  $V$ ,  $\widetilde{\mathbb{C}}$  is also a copula, since this is a joint distribution of marginally uniform variables.

$$\{\widehat{\mathbb{M}}(U) > 1/2 + \epsilon\} = \{\widehat{\mathbb{M}}(V) < 1/2 - \epsilon\}$$

hence by a union bound.

$$\begin{aligned} \mathbb{C}(|\widehat{\mathbb{M}}(U) - 1/2| > \epsilon) &\leq \mathbb{C}(\widehat{\mathbb{M}}(U) < 1/2 - \epsilon) + \widetilde{\mathbb{C}}(\widehat{\mathbb{M}}(V) < 1/2 - \epsilon) \\ &= 2(1/2 - \epsilon) + 2(1/2 - \epsilon) \end{aligned}$$

then clearly since we are dealing with a probability measure.

$$\begin{aligned} \mathbb{C}(|\widehat{\mathbb{M}}(U) - 1/2| > \epsilon) &\leq 2 \max\{1 - 2\epsilon, 0\} \\ &= 2P(|U - 1/2| > \epsilon) \end{aligned}$$

□

**Lemma A.6.** *For any set of marginally identically distributed random variables  $\{X_i\}_{i=1}^n$*

with CDF  $F$  generated with an arbitrary copula  $\mathbb{C}$ , then:

$$P(\widehat{\mathbb{M}}(X) \leq t) \leq 2P(X_1 \leq t) \quad (19)$$

*Proof.* The proof immediately is a result of Lemma A.2 and A.4.

$$\begin{aligned} P(\widehat{\mathbb{M}}(X) \leq t) &= \mathbb{C}(F^{-1}(\widehat{\mathbb{U}}) \leq t) \text{ Lemma A.2} \\ &= \mathbb{C}(\widehat{\mathbb{U}} \leq F(t)) \\ &\leq 2P(U \leq F(t)) \text{ Lemma A.4} \\ &= 2F(t) \\ &= 2P(X_1 \leq t) \end{aligned}$$

□

This concludes the proof of Theorem 2.6

## A.8 Proof of Theorem 2.5

*Proof.* Denote the set of events  $M_i(t) = \widehat{\mathbb{M}}[\Xi(Z_{\{1, \dots, i\}})] > t$  and let  $G = \cap_{i=1}^K M_i(t)$ . We can upper bound the probability that  $\Phi(\mathcal{D}_K) \leq t$  by the following:

$$\begin{aligned} P(\Phi(\mathcal{D}_K) \leq t) &= P(\Phi(\mathcal{D}_K) \leq t | \Phi(\mathcal{D}_{K-1}) \leq t, G) P(\Phi(\mathcal{D}_{K-1}) \leq t | G) P(G) \\ &\quad + P(\Phi(\mathcal{D}_K) \leq t | \Phi(\mathcal{D}_{K-1}) > t, G) P(\Phi(\mathcal{D}_{K-1}) > t | G) P(G) \\ &\quad + P(\Phi(\mathcal{D}_K) \leq t | G^c) P(G^c) \\ &\leq \underbrace{P(\Phi(\mathcal{D}_K) \leq t | \Phi(\mathcal{D}_{K-1}) \leq t, G)}_{(I)} P(\Phi(\mathcal{D}_{K-1}) \leq t | G) + \underbrace{P(G^c)}_{(II)} \end{aligned}$$

We first consider (I). Since we assume  $G$  at each step, at least half of the midpoints are at a distance  $t$  away. Therefore:

$$\begin{aligned}
(I) &= P(\Phi(\mathcal{D}_K) \leq t | \Phi(\mathcal{D}_{K-1}) \leq t, G) \\
&\leq \max\{0, 1 - \binom{K}{2} \alpha \frac{C_p}{2} t^p\} \\
&\leq \exp(-\binom{K}{2} \alpha \frac{C_p}{2} t^p)
\end{aligned}$$

By recursion, we can apply this such that:

$$\begin{aligned}
\prod_{k=1}^K P(\Phi(\mathcal{D}_K) \leq t | \Phi(\mathcal{D}_{K-1}) > t, G) &\leq \exp(-\sum_{k=1}^K \binom{k}{2} \alpha \frac{C_p}{2} t^p) \\
&= \exp(-\binom{K+1}{3} \alpha \frac{C_p}{2} t^p) \\
&\leq \exp(-(K+1)^3 \alpha \frac{C_p}{12} t^p)
\end{aligned}$$

Secondly let we consider term (II). Then

$$\begin{aligned}
P(G^c) &= P(\cup_{k=1}^K \{\widehat{\mathbb{M}}[\Xi(Z_{\{1, \dots, k\}})] \leq t\}) \\
&\leq \sum_{k=1}^K P(\widehat{\mathbb{M}}[\Xi(Z_{\{1, \dots, k\}})] \leq t) \\
&\leq K(P(\widehat{\mathbb{M}}[\Xi(Z_K)] \leq t))
\end{aligned}$$

Since by definition, the median distance to the closest midpoint will be decreasing as we add more points. Next, by Lemma A.4

$$\begin{aligned}
P(\{\widehat{\mathbb{M}}[\Xi(Z_K)] \leq t\}) &\leq 2P(\Xi(Z_K) \leq t) \\
&= 2P(\cup_{m' \neq m} d(m, m') \leq t) \\
&\leq 2 \sum_{m' \neq m} P(d(m, m') \leq t)
\end{aligned}$$

And by assumption in our theorem  $P(d(m, m') \leq t) \leq C_p t^p$ . Hence we combine these bounds

$$P(\Phi(\mathcal{D}_K) \leq t) \leq \exp(-(K+1)^3 \alpha \frac{C_p}{12} t^p) + 2K \binom{K}{2} t^p$$

Letting  $t = \frac{C_2}{K^{3/q}}$  will allow bounding  $P(\Phi(\mathcal{D}_K) \leq t)$  by any constant and therefore:

$$\Phi(\mathcal{D}_K) = \mathcal{O}_P(K^{-3/q})$$

□

## B Additional Computational Details

### B.1 Newton Method for $\hat{\kappa}$

Given a set of distances  $\hat{d}$  we can estimate the curvature using a newton method. Firstly, we compute the derivative of  $g(\kappa, d)$  with respect to  $\kappa$ .

$$\begin{aligned} \frac{\partial}{\partial \kappa} g(\kappa, d) = & (1/(4\kappa^2)) \left( 8 \cos(d_{xm} \sqrt{\kappa}) - 4 \cos(d_{xz} \sqrt{\kappa}) \sec(d_{yz} \frac{\sqrt{\kappa}}{2}) + 4 d_{xm} \sqrt{\kappa} \sin(d_{xm} \sqrt{\kappa}) \right. \\ & - 2 d_{xy} \sqrt{\kappa} \sec(d_{yz} \frac{\sqrt{\kappa}}{2}) \sin(d_{xy} \sqrt{\kappa}) - 2 d_{xz} \sqrt{\kappa} \sec(d_{yz} \frac{\sqrt{\kappa}}{2}) \sin(d_{xz} \sqrt{\kappa}) \\ & + d_{yz} \sqrt{\kappa} \cos(d_{xz} \sqrt{\kappa}) \sec(d_{yz} \frac{\sqrt{\kappa}}{2}) \tan(d_{yz} \frac{\sqrt{\kappa}}{2}) \\ & \left. + \cos(d_{xy} \sqrt{\kappa}) \sec((d_{yz} \sqrt{\kappa})/2) (-4 + d_{yz} \sqrt{\kappa} \tan(d_{yz} \frac{\sqrt{\kappa}}{2})) \right) \end{aligned}$$

This allows us to construct a newton method for estimating the root  $\hat{\kappa}$

$$\widehat{\kappa}_{(m+1)} = \widehat{\kappa}_{(m)} - \frac{g(\widehat{\kappa}_{(m)}, \widehat{d})}{\frac{\partial}{\partial \kappa} g(\widehat{\kappa}_{(m)}, \widehat{d})}$$

### B.1.1 Infeasible midpoint distances

For a known set  $x, y, z, m$  we can estimate the curvature  $\widehat{\kappa}$ . However, since these measurements are in general noisy, there will be times when we observe a distance which cannot correspond to a triangle and midpoint in any canonical geometry. This may happen when the midpoint distance  $\widehat{d}_{xm} > \widehat{d}_{xy}, \widehat{d}_{xz}$ . In this setting, this tends to be a case that the midpoint distance is so large that it cannot be embedded in any spherical geometry, we may have a similar setting when observing  $\widehat{d}_{xm}$  too small for any hyperbolic geometry. For a set of  $\widehat{d}_{xy}, \widehat{d}_{xz}, \widehat{d}_{yz}$  with a known  $\kappa$ , we can always solve for  $\widehat{d}_{xm}$  and taking  $\lim \kappa \pm \infty$  gives an upper and lower bound for  $\widehat{d}_{xm}$ . If we find that the noisy measured distance is outside of that range, then we estimate  $\widehat{\kappa} = \pm\infty$ . The main purpose of this is to reduce the number of steps required until the root is found.

In order to perform a maximum likelihood estimate for the noisy distance matrix, we note that this is a convex problem.

## B.2 Distance Estimation

We recall the problem of estimating a distance matrix from a set of cliques  $\mathcal{C}$ . Though this problem is convex, due to the  $O(K^3)$  restrictions in the problem, it the problem is often slow to reach a solution in CVXR. Instead, we solve this problem using a successive second order approximation.

$$\begin{aligned}
f(D) &:= \sum_{X,Y \in \mathcal{C}, i \in X, j \in Y} A_{ij}(\nu_i + \nu_j - D_{x,y}) + (1 - A_{ij}) \log(1 - \exp(\nu_i + \nu_j - D_{x,y})) \\
&\approx \sum_{X,Y \in \mathcal{C}, i \in X, j \in Y} A_{ij}(\nu_i + \nu_j - D_{0,x,y}) + (1 - A_{ij}) \log(1 - \exp(\nu_i + \nu_j - D_{0,x,y})) \\
&+ \sum_{X,Y \in \mathcal{C}, i \in X, j \in Y} -A_{ij}(D_{x,y} - D_{0,x,y}) - (1 - A_{ij}) \frac{\exp(\nu_i + \nu_j - D_{0,x,y})}{1 - \exp(\nu_i + \nu_j - D_{0,x,y})} (D_{x,y} - D_{0,x,y}) \\
&+ \sum_{X,Y \in \mathcal{C}, i \in X, j \in Y} -(1 - A_{ij}) \frac{\exp(\nu_i + \nu_j - D_{0,x,y})}{(1 - \exp(\nu_i + \nu_j - D_{0,x,y}))^2} \frac{(D_{x,y} - D_{0,x,y})^2}{2} \\
&:= \tilde{g}(D, D_0)
\end{aligned}$$

Hence to compute the global solution  $\hat{D}$ , we can iteratively solve the following optimization problem

$$\begin{aligned}
\hat{D}_{t+1} &= \operatorname{argsup}_{D \in \mathbb{R}^{K \times K}} \tilde{g}(D, \hat{D}_t) \\
D_{ij} &\geq 0 \quad \text{for all } i, j \\
\operatorname{Diag}(D) &= 0 \\
\operatorname{tr}(E_s^T D) &\geq 0 \forall s \in \mathcal{S}
\end{aligned}$$

This process can be further sped up by choosing a good initialization matrix. We can do this by using the unconstrained maximum likelihood estimate  $\hat{D}_U$ , which is very fast to compute but does not enforce triangle inequality restrictions. This can be computed analogously as in theorem 3.4. Though many of the distances  $\hat{D}_U$  may not satisfy the triangle inequality, we can trim the distances so that  $\hat{D}_U$  form a distance matrix, and use this as the starting point. The Floyd-Warshall Algorithm is a possible option for constructing a distance matrix from a noisy matrix which might not have a distance structure. A natural extension to this in our context is as follows.

---

**Algorithm 1:** Adapted Floyd-Warshall Algorithm

---

```
Input  $D : D = D^T$ ;  
Trim entries below 0:  $D[D < 0] \leftarrow 0$ ;  
for  $k \in \{1, 2, \dots, n\}$  do  
  for  $j \in \{1, 2, \dots, n\}$  do  
    for  $i \in \{1, 2, \dots, n\}$  do  
      if  $D_{ij} > (D_{ik} + D_{kj})$  then  
         $D_{ij} \leftarrow (D_{ik} + D_{kj})$ ;
```

---

One can draw similarities here to the problem of sparse metric repair. Metric repair seeks to adjust the fewest entries in a noisy distance matrix so that it still preserves the properties of being a metric (positivity, triangle inequality). Gilbert and Jain (2017) illustrated this Floyd-Warshall algorithm to be a solution to a special type known as decrease only metric repair.

## C Other link functions:

Another common link function is the and formulation of the model is via the following:

$$\begin{aligned}\nu_i &\sim F_\nu, \quad \nu_i \leq 0 \\ Z_i &\sim F_Z, \quad Z_i \in \mathcal{M}^p \\ P(G_{ij} = 1) &= \text{logit}(\nu_i + \nu_j + \varphi - d(Z_i, Z_j))\end{aligned}$$

We can consistently estimate the node level parameters up to a constant shift using conditional maximum likelihood. The parameter  $\varphi$  controls the global sparsity. Similar to before, we note that  $\nu_i$  terms are likely to be very large in a cliques then we can set the largest parameter in each group to be nearly zero.

Questions, how do we estimate  $\varphi$ ? One option would be to let  $\hat{\varphi} = \min(\hat{D})$  and sup-

pose that the smallest distance pair is 0. We know that this typically happens at a rate of  $O_P(K^{-2/p})$  so if there are a number of cliques, that bias should be small.

Other link functions may be used but will likely all need specific methods to estimate  $\nu_i$  parameters within each clique. However, we have shown how it can be developed in these two canonical cases.

## D Riemannian Geometry Definitions

In this section, we review some definitions of the sectional and scalar curvature as well as the volume elements. A Riemannian manifold  $\mathcal{M} = (M, g)$  is a smooth manifold  $M$  equipped with a Riemannian inner product  $g_q$  on the tangent space  $T_q(\mathcal{M})$  at any point  $q \in \mathcal{M}$ ,  $g_q(u, v) : T_q(\mathcal{M}) \times T_q(\mathcal{M}) \mapsto \mathbb{R}$ .

This inner product can be used to define the Riemann curvature tensor at a point  $q \in \mathcal{M}$   $R_q(u, v)w$ , which takes 3 vectors  $u, v, w$  and returns an element of the tangent space

$$R_q(u, v)w : T_q(\mathcal{M}) \times T_q(\mathcal{M}) \times T_q(\mathcal{M}) \mapsto T_q(\mathcal{M})$$

$$R_q(u, v)w := [\nabla_u, \nabla_v]w - \nabla_{[u, v]}w$$

where  $[u, v]$  is the lie bracket of vector fields and  $[\nabla_u, \nabla_v]$  is the commutator of differential operators. The Riemann curvature tensor can be used to define our main quantity of interest, the sectional curvature at a point  $\kappa_q(u, v) : T_q(\mathcal{M}) \times T_q(\mathcal{M}) \mapsto \mathbb{R}$ . The sectional curvature takes two linearly independent elements of the tangent space and maps them to the real line.

$$\kappa_q(u, v) := \frac{g_q(R_q(u, v)v, u)}{g_q(u, u)g_q(v, v) - g_q(u, v)^2}.$$

The sectional curvature is independent of the coordinate system used, but depends only on the linear subspace spanned by  $u, v$ . Furthermore, in the canonical manifolds  $\kappa_q(u, v) = \kappa$  by construction.

From the sectional curvature, we can define the scalar curvature  $S(m)$ ,

$$S(q) := \sum_{i \neq j} \kappa(e_i, e_j)$$

where  $\{e_i\}_{i=1}^p$  form an orthonormal frame for  $T_q(\mathcal{M})$ . We can think of the scalar curvature as an “average of sectional curvatures” across the manifold.

We next define a volume form (also known as the Levi-Civita Tensor) via the Riemannian inner product  $g$ . If  $\omega$  is a local oriented coordinate system near a point  $q$  then

$$dV := \sqrt{|\det(g)|} d\omega.$$

where  $g_q$  is the metric tensor evaluated on the basis coordinate system  $\omega$ . For further details on these quantities, see Klingenberg (1995).

From this definition of a volume, we can define probability density functions on the manifold. A density function  $f$  corresponding to a measure  $F$  with support on the manifold can be defined as follows. For a set  $\mathcal{X} \subset \mathcal{M}$ .

$$P(X \in \mathcal{X}) = \int_{x \in \mathcal{X}} f(x) dV_x$$

See Pennec (1999) for further introduction for defining probabilities on the manifold.

## E Assumptions on $\mathcal{M}$

Here we verify that the Algebraic Midpoint properties, as well as locally Euclidean properties are satisfied for a complete simply connected smooth Riemannian manifolds.

If the algebraic midpoint property is satisfied for any complete metric space  $\mathfrak{M}$  then by Theorem 1.8 of Gromov (2007), then  $\mathfrak{M}$  is a **path metric space**. The authors follow up in discussion a list of examples of path metric spaces, which include Riemannian manifolds with boundary.

Secondly, if  $\mathcal{M}^p$  has scalar curvature at point  $q$ ,  $S(q)$  then

$$\frac{\text{Vol}(B_{\mathcal{M}^p}(\epsilon, q))}{\text{Vol}(B_{\mathbb{E}^p}(\epsilon, q))} = 1 - \frac{S(q)}{6(p+2)}\epsilon^2 + o(\epsilon^3)$$

by Theorem 3.98 of Gallot et al. (2004). Since this holds, then for a latent metric which is generated by distances on a Riemannian manifold, the locally Euclidean volume property will hold.

## F Graph Statistics From Simulations

Columns denote the scale factor used in the simulations.

Table 4:  $\kappa = -2$  graph statistics summary

Scale ( $\rho$ )	0.7	1	2	4
Edge.fraction	0.016 (0.001)	0.012 (0.001)	0.007 (0.001)	0.006 (0)
Max.Degree	341.3 (23.596)	412.29 (26.364)	656.63 (33.954)	1151.415 (49.907)
Mean.Degree	56.726 (5.279)	58.538 (5.351)	73.975 (5.448)	113.546 (7.311)
Distinct.Cliques $\geq \ell$	78.665 (6.955)	53.675 (5.427)	43.515 (4.41)	65.345 (5.926)
Max.Clique.Size	24.215 (4.985)	28.725 (5.494)	NaN (NA)	NaN (NA)
Mean.Degree.Centrality	0.155 (0.009)	0.134 (0.007)	0.107 (0.005)	0.094 (0.003)

Table 5:  $\kappa = -1$  graph statistics summary

Scale ( $\rho$ )	0.7	1	2	4
Edge.fraction	0.017 (0.002)	0.012 (0.001)	0.008 (0.001)	0.006 (0.001)
Max.Degree	343.69 (25.21)	416.825 (28.796)	661.12 (32.257)	1110.87 (141.389)
Mean.Degree	58.943 (5.354)	61.168 (5.636)	78.239 (5.6)	115.484 (15.476)
Distinct.Cliques $\geq \ell$	80.14 (6.488)	54.965 (5.404)	42.32 (5.027)	61.89 (6.009)
Max.Clique.Size	24.005 (5.456)	28.735 (6)	NaN (NA)	NaN (NA)
Mean.Degree.Centrality	0.159 (0.008)	0.137 (0.007)	0.112 (0.005)	0.098 (0.004)

Table 6:  $\kappa = -0.5$  graph statistics summary

Scale ( $\rho$ )	0.7	1	2	4
Edge.fraction	0.017 (0.001)	0.013 (0.001)	0.008 (0.001)	0.006 (0)
Max.Degree	340.785 (21.648)	413.115 (24.818)	656.07 (39.433)	1127.555 (53.421)
Mean.Degree	59.658 (4.776)	62.67 (4.989)	79.873 (6.566)	120.243 (7.558)
Distinct.Cliques $\geq \ell$	80.205 (6.493)	55.155 (5.288)	39.95 (5.289)	58.935 (5.585)
Max.Clique.Size	23.62 (5.216)	29.52 (6.073)	NaN (NA)	NaN (NA)
Mean.Degree.Centrality	0.161 (0.009)	0.141 (0.007)	0.114 (0.005)	0.1 (0.003)

Table 7:  $\kappa = 0$  graph statistics summary

Scale ( $\rho$ )	0.7	1	2	4
Edge.fraction	0.012 (0.001)	0.008 (0)	0.005 (0)	0.004 (0)
Max.Degree	205.38 (16.619)	242.88 (18.178)	371.805 (24.336)	631.745 (35.668)
Mean.Degree	40.815 (2.626)	41.759 (2.415)	52.465 (2.813)	79.593 (3.363)
Distinct.Cliques $\geq \ell$	70.2 (13.19)	46.84 (6.057)	41.54 (4.576)	61.665 (5.926)
Max.Clique.Size	23.735 (5.244)	28.49 (5.421)	41.63 (7.913)	NaN (NA)
Mean.Degree.Centrality	0.169 (0.017)	0.149 (0.013)	0.125 (0.009)	0.114 (0.006)

Table 8:  $\kappa = 0.5$  graph statistics summary

Scale ( $\rho$ )	0.7	1	2	4
Edge.fraction	0.017 (0.001)	0.013 (0.001)	0.008 (0)	0.006 (0)
Max.Degree	267.08 (17.432)	318.615 (18.062)	488.545 (25.046)	825.605 (34.975)
Mean.Degree	61.311 (2.803)	63.539 (2.96)	80.373 (3.454)	123.14 (3.813)
Distinct.Cliques $\geq \ell$	87.945 (12.778)	55.385 (7.343)	39.535 (5.591)	58.425 (6.022)
Max.Clique.Size	23.595 (4.844)	28.45 (6.158)	39.925 (7.861)	NaN (NA)
Mean.Degree.Centrality	0.21 (0.016)	0.183 (0.012)	0.153 (0.008)	0.14 (0.007)

Table 9:  $\kappa = 1$  graph statistics summary

Scale ( $\rho$ )	0.7	1	2	4
Edge.fraction	0.025 (0.001)	0.018 (0.001)	0.012 (0)	0.009 (0)
Max.Degree	351.89 (16.965)	421.36 (18.32)	652.265 (26.131)	1106.435 (32.605)
Mean.Degree	88.331 (3.89)	91.901 (3.805)	117.569 (4.089)	181.022 (4.563)
Distinct.Cliques $\geq \ell$	91.71 (30.245)	64.23 (17.006)	41.765 (4.761)	60.89 (5.493)
Max.Clique.Size	24.07 (5.334)	29.29 (6.259)	40.52 (7.969)	NaN (NA)
Mean.Degree.Centrality	0.241 (0.012)	0.21 (0.01)	0.174 (0.007)	0.159 (0.006)